Brown Boveri Review

11

November 1974, Volume 61 Baden/Switzerland

BROWN BOVERI

165 798.C

Brown Boveri Review

11

November 1974, Volume 61 Baden/Switzerland
p. 477–520

Published by BBC Brown, Boveri & Company, Limited,
CH-5401 Baden/Switzerland
Printed by Buchdruckerei Effingerhof AG, Brugg
Obtainable direct from the publisher

Cover:
Lugano trolleybus

Contents

Page

K. Reichert and N. Leon:
Computation Methods and Models for Investigating the Stability of Large Synchronous Machines 480

U. Kogelschatz, E. Schade and K.-D. Schmidt:
Optical Measuring Techniques as a Diagnostic Aid in Circuit-Breaker Development 488

S. Manzoni:
Fourth Series of Trolleybuses for Lugano 494

P. Salzgeber:
Rectifier Substations for Railways 501

R. Gerber:
Low-Ripple Power Supply for Magnets 508

J. C. Rauch and E. Violi:
Coils with Inorganic Insulation and Their Application in Research Magnets 512

In Brief

G. Sola:
AAS Veritron—A New Range of Three-Phase, Two-Way Static Convertors 517

Computation Methods and Models for Investigating the Stability of Large Synchronous Machines

K. Reichert and N. Leon

Mathematical methods for treating stability problems are examined. Various influencing factors are analysed and pointers for their practical application are derived from the findings.

Introduction

The economic efficiency of power generation increases with the size and capacity of the generators. Interconnected operation of networks allows high-capacity power station units to be used without jeopardizing the security of supply.

The use of powerful generators running at high utilization factors, however, gives rise to increased problems of stability during planning and in service, because the transient reactance X_d' of the generator and the reactance X_{tr} of the unit-connected transformer increase with the power rating, whereas the inertia constant H tends to diminish. The effect of these quantities on stability have been reported on comparatively recently [1, 2].

The aim of the present article is to examine the mathematical models used for dealing with stability problems of large turbogenerators. In particular, the following influences will be investigated:

- Simplification and intentional omissions in the system equations or in the models of synchronous machines
- Generator and network parameters
  inertia constant H
  synchronous reactances X_d, X_q
  transient generator reactance X_d'
  stator resistance R
  reactance of transformer and network X_{tr}, X_n
  site of fault (nature of fault)
  prior load, generator capacity S, load angle

Indications concerning the accuracy of stability studies and pointers to economical methods of calculation are derived from the findings.

Fig. 1 – Inertia constant H of turbogenerator sets as a function of power S (lower limit)

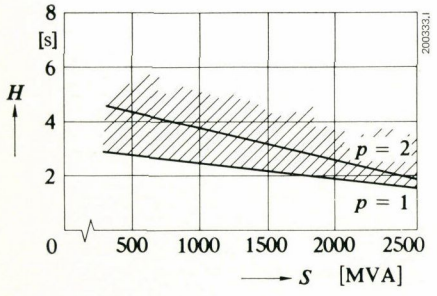

Fig. 2 – Synchronous reactance X_d of turbogenerator as a function of power S
(basis: $X_B = \frac{U^2}{S}$)

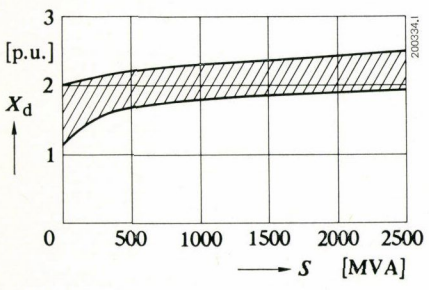

Fig. 3 – Stator resistance R of turbogenerators in relation to power S

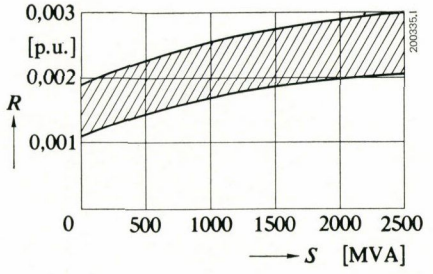

Fig. 4 – Short-circuit time constant T_d' of turbogenerators in relation to power S

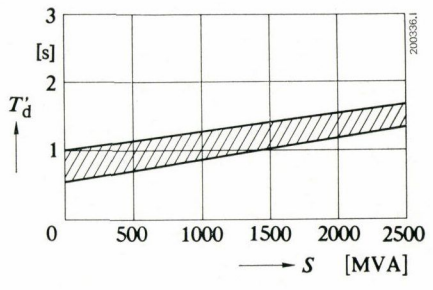

Parameters for Stability Investigations

The major parameters for studying stability are

a. the generator parameters
   H, X_d, X'_d, X''_d, X_q, (X'_q), X''_q, T'_d, T''_d, (T'_q), T''_q, X_p, X_{re}, $E = f(I_F)$
b. the transfer functions of the voltage regulator and turbine controller
c. the unit-transformer reactance X_{tr} and the network
d. the nature of the fault (1-phase, 3-phase, short circuit, etc.), the fault location and fault time t_F

The generator parameters are determined by the construction of the machine. Evaluating the data of a variety of machines, one finds the following trend:

The inertia constant H diminishes with increasing power S and decreasing number of pole pairs p (cf. Fig. 1) [2]:

$$H = \frac{GD^2}{4} \frac{\omega_S^2}{2S} \qquad (1)$$

Here, $\omega_S = 2\pi \times f/p = 2\pi \times n_s$ is the synchronous angular velocity, and $GD^2/4$ the moment of inertia referred to diameter.
Only a lower limit can be stated for inertia constant H because its magnitude is very much influenced by the turbine.
The reactances X_d (Fig. 2) and X'_d (Fig. 5), the stator resistance R (Fig. 3) and the short-circuit time constant T'_d (Fig. 4) similarly show a tendency to become larger with increasing power rating. However, these relationships can be very strongly influenced by structural features and design layout.

Data of the System Models Investigated

Figures 1 to 6 show that the problem spectrum can be covered by a few characteristic system models. The data of these models are presented in Table I.
The generators are connected to an infinite power system via a transformer and a network reactance X_n (single-machine problem).
Generally, when investigating stability, one examines the consequences of the following disturbances:

– Short circuit (1 to 3-phase) in the network with subsequent complete (3-phase) or partial interruption of the load flow between generator and network (rapid reclosure).
– Partial or complete interruption of load flow between generator and network (load rejection).
– Small fluctuations in the load flow (static stability).

Experience shows that the method of calculation and the model influence the results more strongly with high-speed transients than with slow ones, and therefore the following examination concerns only cases of stability with three-phase short circuits between the transformer and the infinite network under different initial conditions. The duration of the short circuit was so chosen that the stability limit was reached in each case.
In order to distinguish more clearly the differences with regard to stability in the various synchronous machine models, the effects of the voltage regulator and turbine controller were not considered when simulating the behaviour with respect to time, i.e. simulation was carried out with constant excitation voltage and torque.

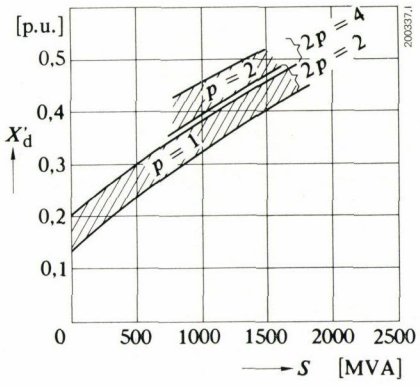

Fig. 5 – Transient reactance X_d' of turbogenerators in relation to power S

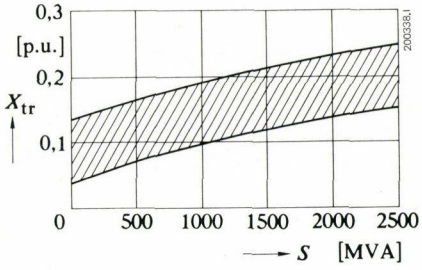

Fig. 6 – Transformer reactance X_{tr} in relation to power S

The Various Synchronous Machine Models

Six different models of synchronous machines were investigated (see Appendix). Saturation was disregarded with all models. The same equations of motion were used for all the models.
Synchronous machine model 1 has three damper windings. The transformational terms in Park's equations and in the network equations (3) are considered.

Table I

		Turbogenerator $S = 30$ MVA	Turbogenerator $S = 600$ MVA	Turbogenerator $S = 1500$ MVA	Hydro-generator $S = 150$ MVA
$p =$		1	1	1	21
R	[p.u.]	0·002	0·0018	0·00205	0·00254
X_c	[p.u.]	0·2	0·188	0·279	0·1
X_d	[p.u.]	1·90	2·0	2·2	0·91
X_q	[p.u.]	1·65	1·85	2·1	0·66
X'_d	[p.u.]	0·238	0·29	0·44	0·30
X''_d	[p.u.]	0·138	0·25	0·324	0·24
X'_q	[p.u.]	–	0·52	0·64	–
X''_q	[p.u.]	0·180	0·23	0·282	0·27
T'_d	[s]	0·76	0·85	1·21	1·1
T'_q	[s]	–	0·58	0·47	–
T''_d	[s]	0·03	0·028	0·03	0·05
T''_q	[s]	0·0584	0·058	0·049	0·06
H	[s]	5·29	3·6	2·65	3·56
X_{tr}	[p.u.]	0·11	0·15	0·20	0·12
X_N	[p.u.]	0·02	0·05	0·10	0·04

In Eq. (3), R_e, L_e is the resistance or inductance of the positive-sequence system between generator and infinite network, i.e. $\omega L_e = X_{tr} + X_N$.

If the site of the short circuit is between the generator and the infinite network, there are ten first-order differential equations to integrate (see Appendix). The time step for integration must be of the order of 0·001 to 0·0005 s.

Synchronous machine model 2 also takes account of the transformational terms, but has only two damper windings. In this case only nine differential equations have to be integrated.

Synchronous machine model 3 also has two damper windings. The transformational terms are disregarded. There are only five differential equations to integrate. It is found from experience that with this configuration the time step can be much larger than with models 1 and 2.

Synchronous machine model 4 has no damper windings. The transformational terms are disregarded. Thus only three differential equations need to be integrated.

Synchronous machine model 5 has no damper windings and no field winding. On the stator side, conditions are represented by one winding each in the direct and quadrature

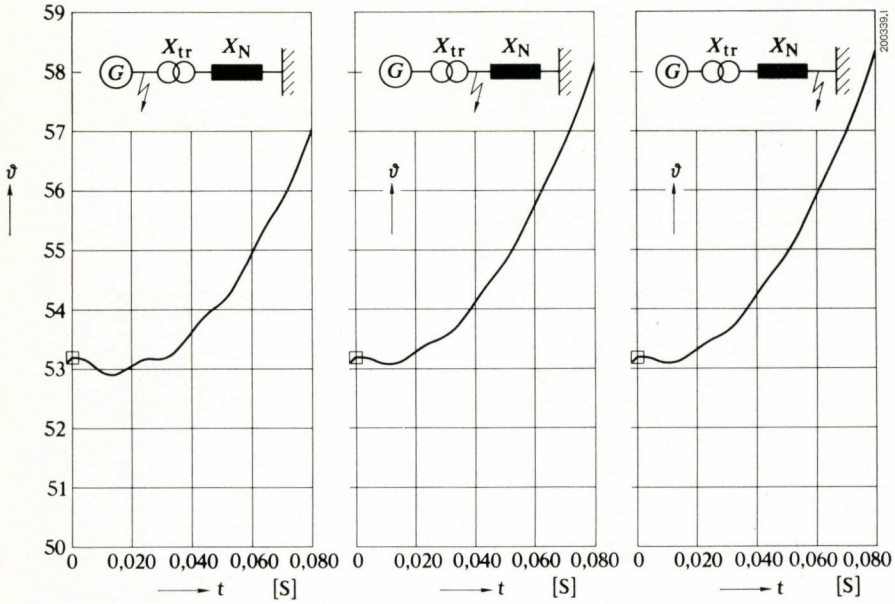

Fig. 7 – Rotor angle ϑ (t) following a short circuit at different locations
$S = 600$ MVA, $p = 1$, $X_{tr} = 0{\cdot}5$, $X_N = 0{\cdot}05$, Model 2

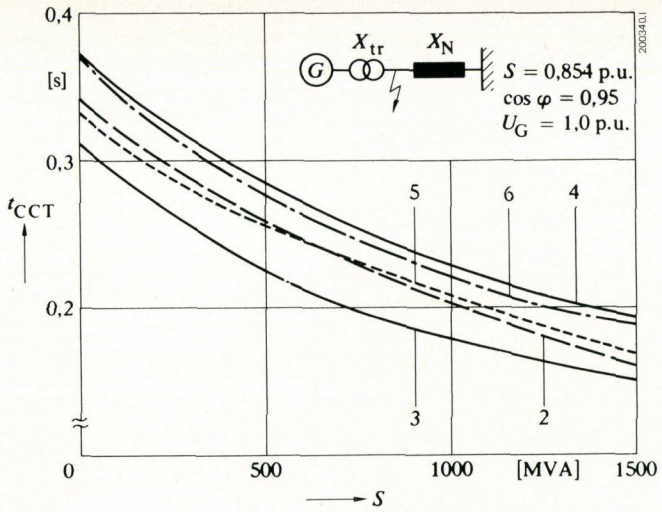

Fig. 8 – Critical short-circuit duration t_{CCT} in case *A* as a function of generator power *S* for different synchronous machine models (2 to 6)

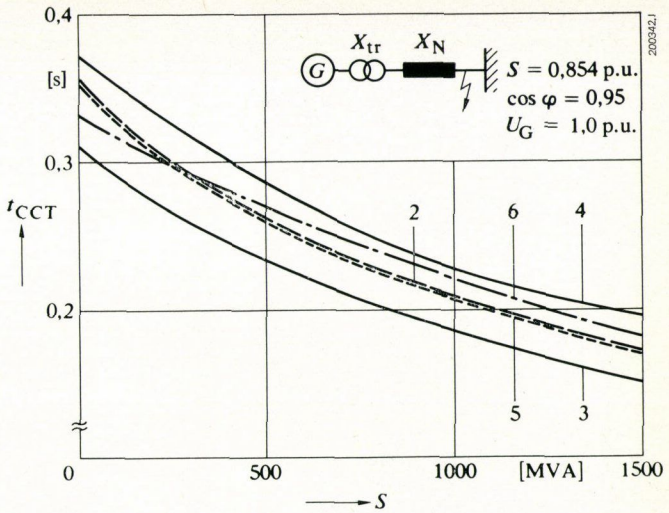

Fig. 10 – Critical short-circuit duration t_{CCT} in case *C* as a function of generator power *S* for different synchronous machine models (2 to 6)

axes, their reactances being of different values. The effect of excitation appears as a current source in the equivalent circuit of the direct-axis winding. Only the two differential equations for the mechanical system have to be integrated.

Synchronous machine model 6 is of the same structure as model 5 except that it has identical reactances in the direct axis and quadrature axis.

The essential difference between models 1, 2, on the one hand, and 3, 4, 5 and 6, on the other, is the allowance made for the transformational effect. Models 1, 2 and 3 have damper windings, while models 4, 5 and 6 do not.

The stability of a synchronous machine after disconnection of the short circuit is determined chiefly by the accelerating torque M_A, or braking torque M_B, which had been acting on the rotor during the short circuit. Accelerating torque

Fig. 9 – Critical short-circuit duration t_{CCT} in case *B* as a function of generator power *S* for different synchronous machine models (1 to 6)

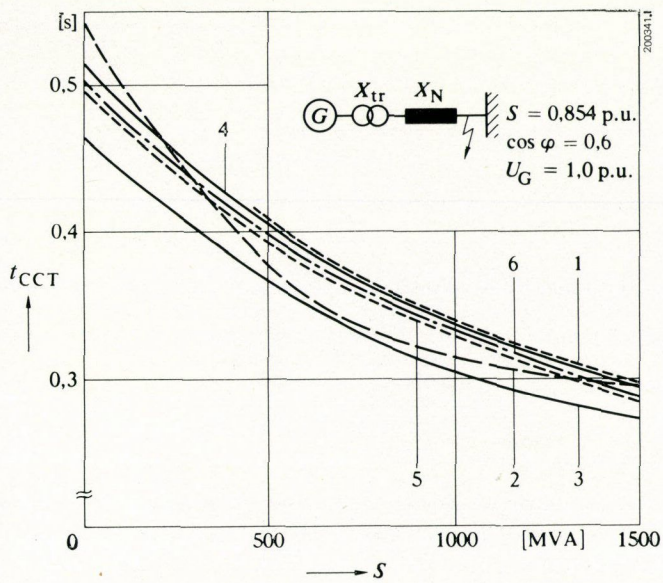

M_A is composed of driving torque M and braking torque M_B:

$$M_A = M - M_B \qquad (2)$$

The braking torque M_B arising during the short circuit and the oscillations, must therefore be correctly represented in each model.

The braking torque M_B acting after the fault has occurred consists of the following component parts (see Appendix):

1. a braking torque M_{B1} corresponding to losses in the stator resistance and network resistance *R*,
2. an asynchronous braking torque M_{B2} corresponding to losses in the rotor windings (field and damper windings),
3. a decaying braking torque M_{B3} introduced by the transformational terms in the machine and network equations. This torque becomes effective at every change of state.

Braking torque M_{B3} is mainly responsible for the well known 'backswing' effect. The synchronous machine is then braked initially in the first 20 ms after the short circuit (cf. Fig. 7). However, as can be seen from Fig. 7, the extent of the backswing is very much dependent on the site of the short circuit, because torque M_{B3} incorporates the network reactances between the machine and short-circuit location. In some instances, therefore, a short circuit across the terminals may be less of a problem as regards stability than a distant short circuit.

Direct account is taken of braking torques M_{B1} to M_{B3} only in the case of models 1 and 2. Braking torque M_{B1} is present with all the models. With model 3 there is also torque M_{B2}.

Investigations and Results

The stability of the synchronous machines described in Table I was investigated as a single-machine problem. The critical short-circuit duration t_{CCT} was taken as a criterion

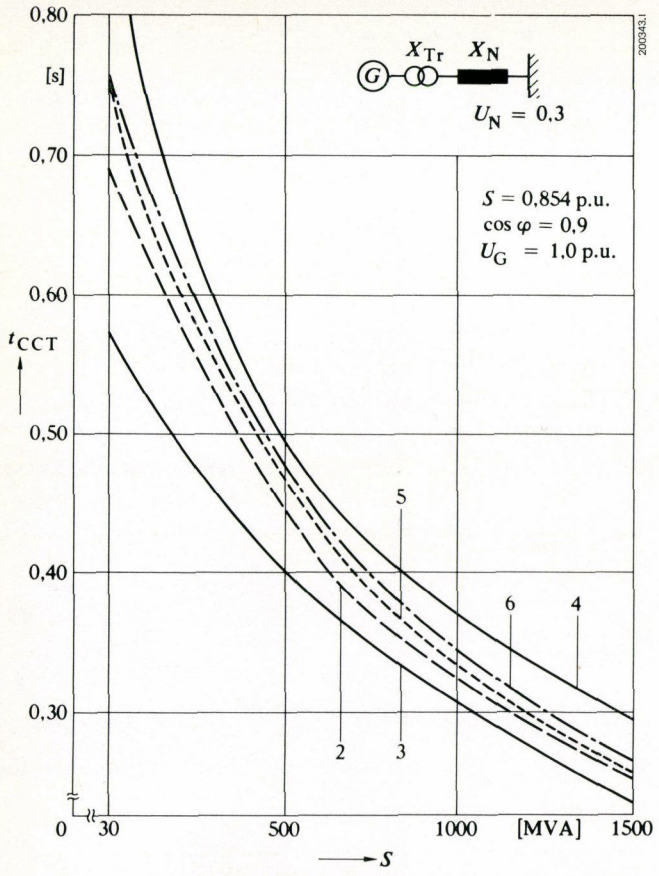

Fig. 11 – Critical short-circuit duration t_{CCT} in case D as a function of generator power S for different synchronous machine models (2 to 6)

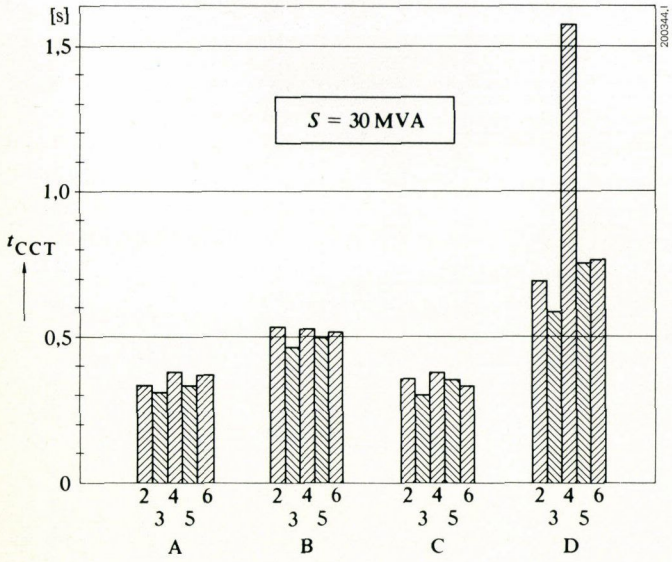

Fig. 12 – Critical short-circuit duration t_{CCT} with different network situations (A, B, C, D) for a power of S = 30 MVA (p = 1)
2 to 6 = Models

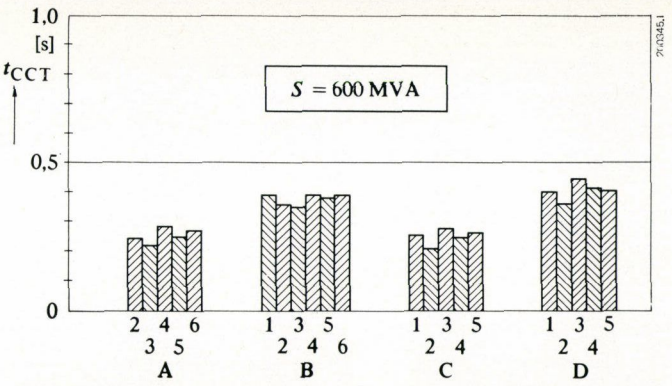

Fig. 13 – Critical short-circuit duration t_{CCT} with different network situations (A, B, C, D) for a power of S = 600 MVA (p = 1)
1 to 6 = Models

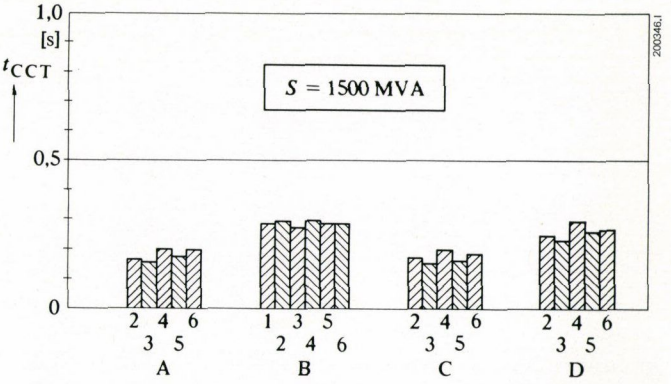

Fig. 14 – Critical short-circuit duration t_{CCT} with different network situations (A, B, C, D) for a power of S = 1500 MVA (p = 1)
1 to 6 = Models

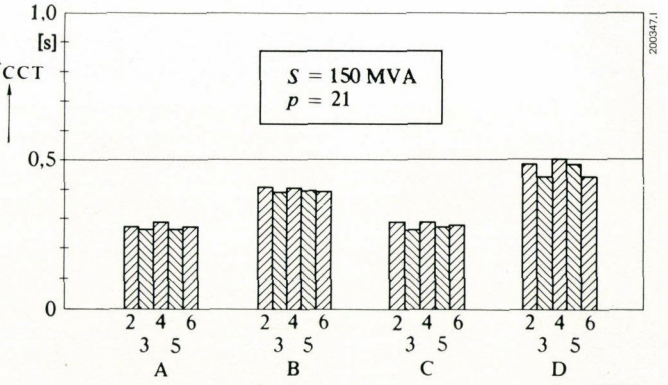

Fig. 15 – Critical short-circuit duration t_{CCT} with different network situations (A, B, C, D) for a power of S = 150 MVA (p = 21)
2 to 6 = Models

for comparing the correctness of the various models. The location of the short-circuit and the initial conditions (S, cos φ) were varied in order to establish the influence of these quantities (cf. configurations in Fig. 8 to 11).
The rotor angle with respect to time of a turbogenerator rated at S = 1500 MVA, as calculated with different models, is shown in Fig. 16.

The following conclusions can be drawn from these results:

1. The transformational terms in the Park's equations (models 1 and 2) and in the network equations must be taken into account

- when power is low,
- when the short circuit is in the vicinity of the generator,
- if the braking torque M_{B3} brought about by the transformational terms cannot be introduced into the mechanical equations.

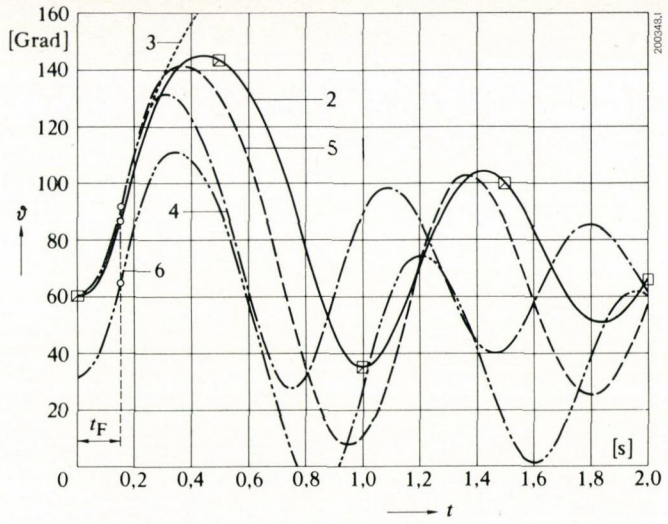

Fig. 16 – Rotor angle $\vartheta(t)$ in case A for $S = 1500$ MVA ($p = 1$), $X_{tr} = 0{\cdot}2$, $X_N = 0{\cdot}1$, $t_f = 0{\cdot}155$s

2. The backswing effect occurs only when the site of the short circuit is close to the generator. From this it follows that under certain circumstances a short circuit remote from the generator can be more dangerous, as regards stability, than one nearby.

3. It is shown that the individual synchronous machine models behave very differently.

In many instances, especially in the case of transient stability problems, the simpler models (4 and 5) exhibit the same behaviour as model 2 or 1 with transformational effect. Nevertheless, with the simple models it is particularly important to represent damping correctly.
Models 4 and 5 are therefore particularly suitable for simulating synchronous machines with constant excitation voltage which are located far away from the short circuit.
The investigation shows also that the widely recommended model 6 (constant voltage beyond transient reactance) yields results which are too pessimistic.
If it is assumed that constant H decreases, and reactances X_d, X'_d and X_t increase, with rising generator capacity, then the critical short-circuit duration will be smaller as generator capacity rises. These studies show, however, that the behaviour of even large synchronous machines can be described with the known models of synchronous machines, and that there is usually no need to make allowance for the transformational terms. The result, as Table II shows, is a substantial saving in computer time, which is of particular benefit when studying the stability of multiple-machine configurations.

Table II

Model No.	1	2	3	4	5 and 6
Computer time in seconds for 2 s of real time (IBM 370/155)	32	30	9	7	5·8

Bibliography

[1] *C. Concordia, P. G. Brown:* Effects of trends in large steam turbine driven generator parameters on power system stability. IEEE Trans. Pwr Appar. & Syst. *90* 1971 2211–2218.

[2] *H. E. Lokay, P. O. Thoits:* Effects of future turbine-generator characteristics on transient stability. IEEE Trans. Pwr Appar. & Syst. *90* 1971 2427–2431.

[3] *M. Canay:* Causes of discrepancies on calculation of rotor quantities and exact equivalent diagrams of the synchronous machine. IEEE Trans. Pwr Appar. & Syst. *88* 1969 1114–1120.

[4] *J. L. Dinley, A. J. Morris:* Synchronous generator transient control. Part I: Theory and evaluation of alternative mathematical models. Proc. PICA 1971 182–190.

Appendix

Description of the Synchronous Machine Models

Model 1

This model has six windings. Its equivalent diagram is shown in Fig. 17.
The corresponding equations are:

Network equations

$$\left.\begin{aligned} U_d^G &= U_d^N + R_e i_d + L_e \times di_d/dt - \omega L_e i_q \\ U_q^G &= U_q^N + R_e i_q + L_e \times di_d/dt + \omega L_e i_d \end{aligned}\right\} \qquad (3)$$

in which $L_e = X_{tr} + X_N$.

Fig. 17 – Equivalent circuit of model 1 of a synchronous machine
For symbols, see text.

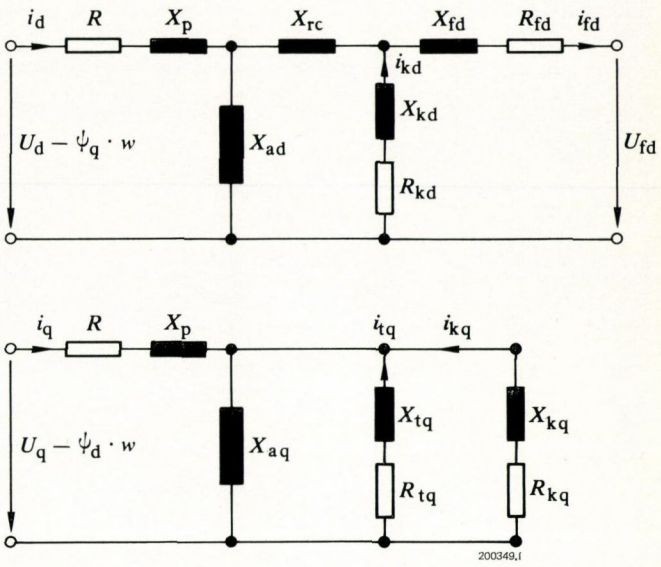

Flux/current relationships

$$\left.\begin{aligned}
\psi_d &= (X_p + X_{ad})\, i_d + X_{ad}\, i_{kd} - X_{ad}\, i_{fd} \\
\psi_{fd} &= -X_{ad} i_d - (X_{ad} + X_{rc}) i_{kd} + (X_{ad} + X_{rc} + X_{fd}) i_{fd} \\
\psi_{kd} &= X_{ad}\, i_d + (X_{ad} + X_{rc} + X_{kd}) i_{kd} - (X_{ad} + X_{rc}) i_{fd} \\
\psi_q &= (X_p + X_{aq})\, i_q + X_{aq}\, i_{tq} + X_{aq}\, i_{kq} \\
\psi_{tq} &= X_{aq}\, i_q + (X_{aq} + X_{tq})\, i_{tq} + X_{aq}\, i_{kq} \\
\psi_{kq} &= X_{aq}\, i_q + X_{aq}\, i_{tq} + (X_{aq} + X_{kq})\, i_{kq}
\end{aligned}\right\} \quad (4)$$

Voltage equations

$$\left.\begin{aligned}
d\psi_d/dt &= -U_d^G + \psi_q \times \omega - R i_d \\
d\psi_q/dt &= -U_q^G - \psi_d \times \omega - R i_q \\
d\psi_{fd}/dt &= U_{fd} - R_{fd}\, i_{fd} \\
d\psi_{tq}/dt &= -R_{tq}\, i_{tq} \\
d\psi_{kd}/dt &= -R_{kd}\, i_{kd} \\
d\psi_{kq}/dt &= -R_{kq}\, i_{kq}
\end{aligned}\right\} \quad (5)$$

Mechanical equations

Torque:

$$M_B = \psi_q i_d - \psi_d\, i_q \quad (6)$$

Power:

$$P = U_d^G\, i_d + U_q^G\, i_q \quad (7)$$

$$Q = U_q^G\, i_d - U_d^G\, i_q \quad (8)$$

Equation of motion:

$$2H \frac{ds}{dt} = M - M_B \quad (9)$$

$$\frac{d\vartheta}{dt} = s \quad (10)$$

$$\omega = 1 + s \quad (11)$$

The quantities L, X, R, φ, i, U, M and ω are per-unit quantities.

From the input data:

R, X_p, X_c, X_d, X_q, X'_d, X''_d, X''_q, T'_d, T'_q, T''_d and T''_q, S_N, U_N, f, I_{fd_0}, U_{fd_0}, p, H

of which T, S_N, U_N, f, I_{fd_0}, U_{fd_0} and H are not in p.u., the constants X_{ad} and X_{aq} of the synchronous machine can be calculated in the following manner:

$$X_{ad} = X_d - X_p \quad (12)$$

$$X_{aq} = X_q - X_p \quad (13)$$

$$X_{rc} = \frac{X_{ad}(X_{rc} - X_p)}{X_d - X_{rc}} \quad (14)$$

$$X_{fd} = \left(\frac{X_d - X_p}{X_d - X_{rc}}\right)^2 \frac{(X_d - X_c)(X'_d - X_c)}{X_d - X'_d} \quad (15)$$

$$X_{kd} = \left(\frac{X_d - X_p}{X_d - X_{rc}}\right)^2 \frac{(X'_d - X_c)(X''_d - X_c)}{X'_d - X''_d} \quad (16)$$

$$X_{tq} = \frac{(X_q - X_p)(X'_q - X_p)}{X_q - X'_q} \quad (17)$$

$$X_{kq} = \frac{(X'_q - X_p)(X''_q - X_p)}{X'_q - X''_q} \quad (18)$$

$$R_{fd} = \left(\frac{X_d - X_p}{X_d - X_{rc}}\right)^2 \frac{(X_d - X_c)^2}{X_d - X'_d} \frac{1}{T_{fd}\, \omega_B} \quad (19)$$

$$R_{kd} = \left(\frac{X_d - X_p}{X_d - X_{rc}}\right)^2 \frac{(X'_d - X_c)^2}{X'_d - X''_d} \frac{X''_d}{T''_d\, X'_d\, \omega_B} \quad (20)$$

$$R_{kq} = \frac{(X'_q - X_p)^2}{X'_q - X''_q} \frac{X''_q}{T''_q\, X'_q\, \omega_B} \quad (21)$$

$$R_{tq} = \frac{(X_q - X_p)^2}{X_q - X'_q} \frac{1}{T_{tq}\, \omega_B} \quad (22)$$

$$T_{fd} = T'_d \frac{X_d}{X'_d} - \left(T_{kd} - T''_d \frac{X'_d}{X''_d}\right) \quad (23)$$

where

$$\left.\begin{aligned}
T_{kd} &= T''_d \frac{X'_d}{X''_d} \times \\
&\times \frac{(X_d - X_{rc})(X'_d - X''_d) + (X'_d - X_{rc})(X''_d - X_{rc})}{(X'_d - X_{rc})^2}
\end{aligned}\right\} \quad (24)$$

$$T_{tq} = T'_q \frac{X_q}{X'_q} - \left(T_{kq} - T''_q \frac{X'_q}{X''_q}\right) \quad (25)$$

$$\left.\begin{aligned}
T_{kq} &= T''_q \frac{X'_q}{X''_q} \times \\
&\times \frac{(X_q - X_p)(X'_q - X''_q) + (X'_q - X_p)(X''_q - X_p)}{(X'_q - X_p)^2}
\end{aligned}\right\} \quad (26)$$

$$\omega_B = 2\pi f \quad (27)$$

The reference values are:

U_N for voltages U_d^G and U_q^G

S_N for powers P and Q

$I_N = \dfrac{S_N}{\sqrt{3}\, U_N}$ (28) for currents i_d and i_q

$M_N = \dfrac{S_N}{\omega_B}$ (29) for torque M

I_{fd_0} for excitation current i_{fd}

U_{fd_0} for the excitation voltage

Model 2

This model has only one damper winding in the quadrature axis, i.e. $i_{tq} = 0$. The relationships $\psi_{tq} = f(i_q, i_{tq}, i_{kq})$ in Eq. (4) and $p\psi_{tq} = R_{tq}\, i_{tq}$ in Eq. (5) do not apply.

Instead of Eq. (18) and (21) we have:

$$X_{kq} = \frac{(X_q - X_p)(X''_q - X_p)}{X_q - X''_q} \quad (18a)$$

$$R_{kq} = \frac{(X_q - X_p)^2\, X''_q}{(X_q - X''_q)\, T''_q\, X_q \times \omega_B} \quad (21a)$$

Eq. (22), (25) and (26) do not apply.

Model 3

This model, like model 2, has one damper winding in each of the direct and quadrature axes. The transformational terms in the stator equations do not apply, i.e. Eq. (5) becomes:

$$\left.\begin{aligned}
U_d^G &= \psi_q\, \omega - R\, i_d \\
U_q^G &= -\psi_d\, \omega - R\, i_q \\
d\psi_{fd}/dt &= U_{fd} - R_{fd}\, i_{fd} \\
d\psi_{kd}/dt &= -R_{kd}\, i_{kd} \\
d\psi_{kq}/dt &= -R_{kq}\, i_{kq}
\end{aligned}\right\} \quad (5a)$$

The equations of motion (9) to (11) remain unchanged. In addition to M_B in Eq. (6), however, the braking torque M_{B3}, caused by the transformational terms when switching operations occur, must be introduced into Eq. (9):

$$2H\frac{ds}{dt} = M - M_B - M_{B3} \tag{9a}$$

if the movement process is to be represented correctly.

Model 4

This model has no damper windings. The basic equations therefore become:

$$\left.\begin{aligned} \psi_d &= (X_p + X_{ad})\, i_d - X_{ad}\, i_{fd} \\ \psi_{fd} &= -X_{ad}\, i_d + (X_{ad} + X_{fd})\, i_{fd} \\ \psi_q &= (X_p + X_{aq})\, i_q \end{aligned}\right\} \tag{4b}$$

$$\left.\begin{aligned} U_d^G &= \psi_q\, \omega - R\, i_d \\ U_q^G &= -\psi_d\, \omega - R\, i_q \\ d\psi_{fd}/dt &= U_{fd} - R_{fd}\, i_{fd} \end{aligned}\right\} \tag{5b}$$

Since model 4 has no damper windings, the asynchronous damping torque M_{B2} would also have to be included in equation of motion (9):

$$2H\frac{ds}{dt} = M - M_B - M_{B3} - M_{B2} \tag{9b}$$

Instead of Eq. (12) to (26) we have the expressions:

$$X_{ad} = X_d - X_p \tag{12}$$

$$X_{aq} = X_q - X_p \tag{13}$$

$$X_{fd} = \frac{(X_d - X_p)\,(X'_d - X_p)}{X_d - X'_d} \tag{15c}$$

$$R_{fd} = \frac{X_d - X_p}{X_d - X'_d}\,\frac{X'_d}{T'_d\, X_d\, \omega_B} \tag{19c}$$

Model 5

This model has no field winding and no damper winding. The base equations for this model are:

$$\left.\begin{aligned} \psi_d &= X'_d\, i_d - E_f \\ \psi_q &= X_q\, i_q \end{aligned}\right\} \tag{4d}$$

$$\left.\begin{aligned} U_d^G &= \psi_q\, \omega - R\, i_d \\ U_q^G &= -\psi_d\, \omega - R\, i_q \end{aligned}\right\} \tag{5d}$$

The mechanical circumstances are described by Eq. (6), (9), (10) and (11).

E_f is calculated in terms of the initial values of i_d, i_q and U_q^G:

$$E_f = U_q^G + R\, i_q + X'_d\, i_d \tag{30}$$

Model 6

This model, like model 5, has no field winding or damper winding. Eq. (4d) contains X'_d instead of X_q. Thus Eq. (6) becomes

$$M_B = E_f \times i_q$$

The network equations for models 3, 4, 5 and 6 are:

$$\left.\begin{aligned} U_d^G &= U_d^N + R_e\, i_d - \omega\, L_e\, i_q \\ U_q^G &= U_q^N + R_e\, i_q + \omega\, L_e\, i_d \end{aligned}\right\} \tag{3b}$$

Optical Measuring Techniques as a Diagnostic Aid in Circuit-Breaker Development

U. Kogelschatz, E. Schade and K.-D. Schmidt

The ever more stringent requirements to be met by high-voltage circuit-breakers create a need for not only continually improved test methods, but also measuring techniques for observing and analysing events in the region of the breaker contacts. A number of specialized optical measuring methods are described, and their use in switchgear development is illustrated by examples. The various techniques are employed either for investigating the intrinsic light of the arc (high-speed cameras, streak photography, spectroscopy) or in visualizing density variations in the gas by means of a separate light source (schlieren photography, differential interferometry, holography).

Introduction

The development and optimizing of circuit-breakers today requires extremely detailed measuring routines. Overall measurements of current and voltage with high time resolution [1] are by themselves not sufficient to reveal the physical reasons for the ultimate breaking capacity of a breaker design. Furthermore, only through a knowledge of the physical processes is it possible to devise new, efficient switching techniques. It is therefore understandable that the fields of plasma physics and gas dynamics are increasingly providing the switchgear design engineer not only with theoretical model concepts [2], but also with specialized methods of measurement, which are then developed further. These are mainly optical methods which either accurately analyse the intrinsic light of the arc, or use external, very intense light sources (lasers). In a modern switchgear testing station the visitor is surprised to see the equipment under test surrounded by optical measuring apparatus which one would otherwise associate with a wind tunnel or a fusion experiment. For observation purposes the circuit-breakers, etc., are provided with windows so arranged, of course, that they do not affect the contact region, and in particular the gas flow. That this effort and expense is really necessary and justified is shown below with reference to some examples from Brown Boveri's test facilities.

Investigations of Intrinsic Light

Optical studies of the intrinsic light are aimed at answering such questions as:

- Does the arc remain stably on the axis of the nozzle configuration, or does it wander about erratically?
- Does the arc burn in turbulent flow?
- Does the arc diameter conform to calculation [2]?
- Where do the arc roots form, and do they move?
- At what moment does a nozzle cease to be clogged, and how does the arc then behave?
- Where do dielectric breakdowns occur?
  Does this happen in the original, still incompletely cooled arc channel, or can breakdown take place along another dielectrically weakened path?
- How great is contamination due to vapourized metal?
- How high are the arc temperatures?

The first technique to consider is high-speed photography, using framing cameras such as the Dynafax or Fastax which can take pictures of the arc at speeds up to some 35 000 exposures per second. This method is useful if the arc is to be observed at several places simultaneously. A drawback, however, is that the minimum time of 30 μs between successive exposures is still too long to follow the events at current zero, for instance, or when dielectric breakdown occurs. On the other hand, streak cameras, usually of the drum kind for these tests, operate continuously. With this technique an arc cross-section is projected on to a film mounted on a rapidly revolving drum, and so leaves a 'streak' across the film. The cross section under investigation is selected by a slit aperture referred to as the streak slit (Fig. 1). The result is thus a continuous record of the arc diameter at a fixed axial position. The maximum duration of the recording is limited by the time for one revolution of the drum. If the arc is to be observed at several axial positions simultaneously, it is best to record several traces on one film. Fig. 1 shows a drum camera arrangement for recording two sections of arc at once. With this layout, which has been used in studies of the ELK puffer-type breaker [3], two traces are recorded simultaneously on the drum-mounted film. If the extinction chamber vibrates during the switching operation it is advisable to pass the light from the arc to the camera by way of a fibre optics bundle.

To illustrate the streak technique, Fig. 2 shows two photographs of dielectric restriking. The time axis runs from left to right. In both pictures one can see clearly how the arc diameter decreases as the current decays, and the arc extinguishes at current zero. However, after an interval of about 1 ms the recovery voltage can no longer be held. In case 'a', breakdown occurs along the old arc channel, while in case 'b' restriking takes place via the surface of the insulating nozzle. Although the causes of these flashovers are quite different, and therefore naturally require

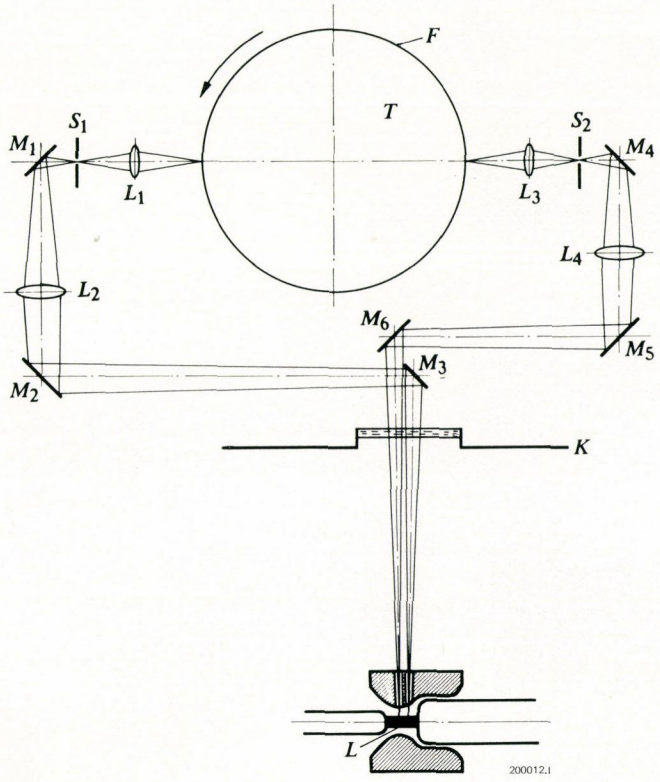

Fig. 1 – Basic layout of streak camera for continuous simultaneous photography of arc diameter at two different axial positions
M_{1-6} = Mirrors
L_{1-4} = Lenses
$S_{1,2}$ = Streak slits
T = Fast rotating drum
F = 36 mm film
K = Breaker enclosure with observation window
L = Arc

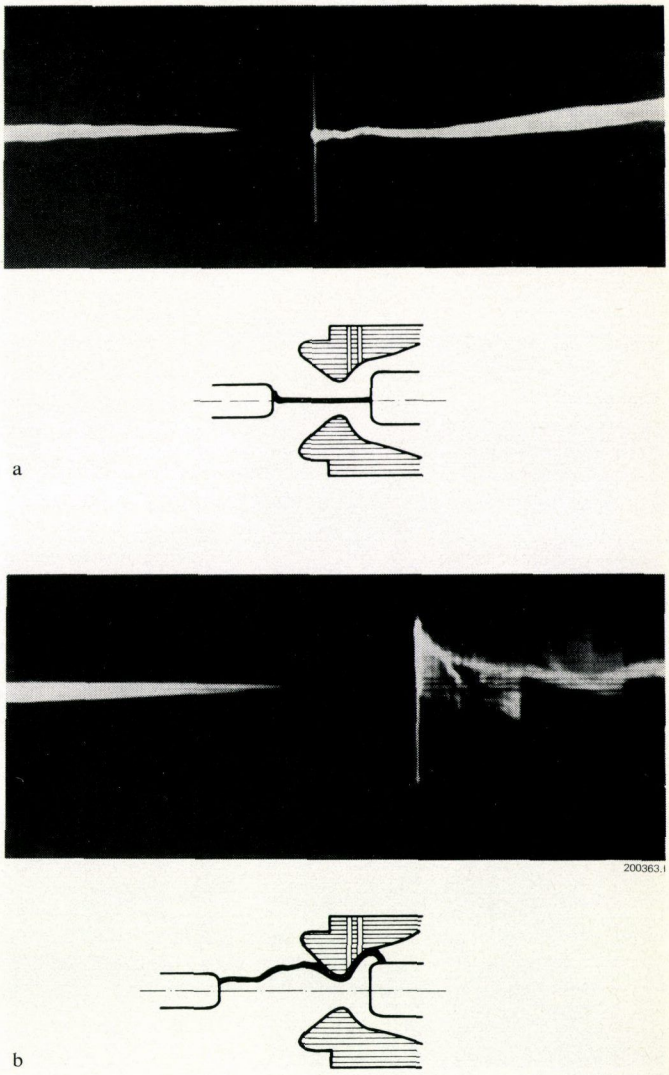

Fig. 2 – Streak photos of dielectric restriking (a) in original discharge channel and (b) over surface of insulating nozzle. The time axis runs from left to right.

quite different design countermeasures, such instances of restriking cannot be distinguished with the aid of voltage measurements. This example thus demonstrates the necessity of optical diagnostic techniques in the optimizing of switchgear.

So far we have considered ways of examining the 'geometry' of the arc, such as position, diameter, etc. Further information can be obtained by splitting up the light of the arc with a spectrograph (Fig. 3) and measuring the light intensity at certain wavelengths. Using plasma spectroscopy it is possible to study the composition of the plasma with respect to contaminants, and establish the temperatures in the arc as a function of distance from the arc axis. This latter point is particularly important when verifying theoretical findings [2].

Investigations with External Light Sources

Also outside the luminous plasma column, physical events occur which can have a vital influence on the breaking capacity. Besides eddies in the gas stream one is especially interested in flow transients after valves have opened. Since these phenomena are accompanied by density variations in the gas stream they can be made visible by schlieren photography. With this technique one makes use of the fact that a beam of light passing through an optically inhomogeneous medium (non-uniform density distribution) is deflected slightly from its original path. With a schlieren diaphragm and a special optical beam configuration the zones of greater density variation can be made to appear dark or light against a uniform background. The

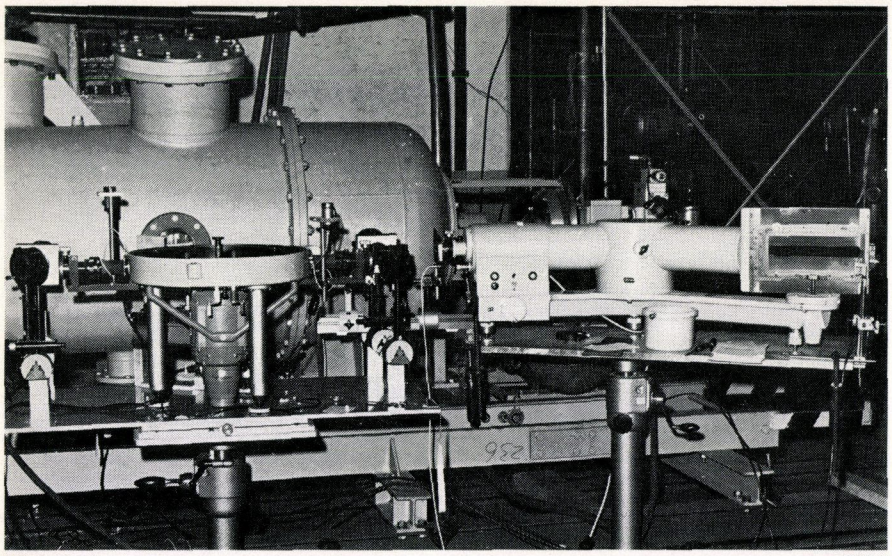

BROWN BOVERI 165734 I

Fig. 3 – Optical apparatus with streak camera (left) and spectrograph (right) on a type ELK puffer-type SF_6 circuit-breaker

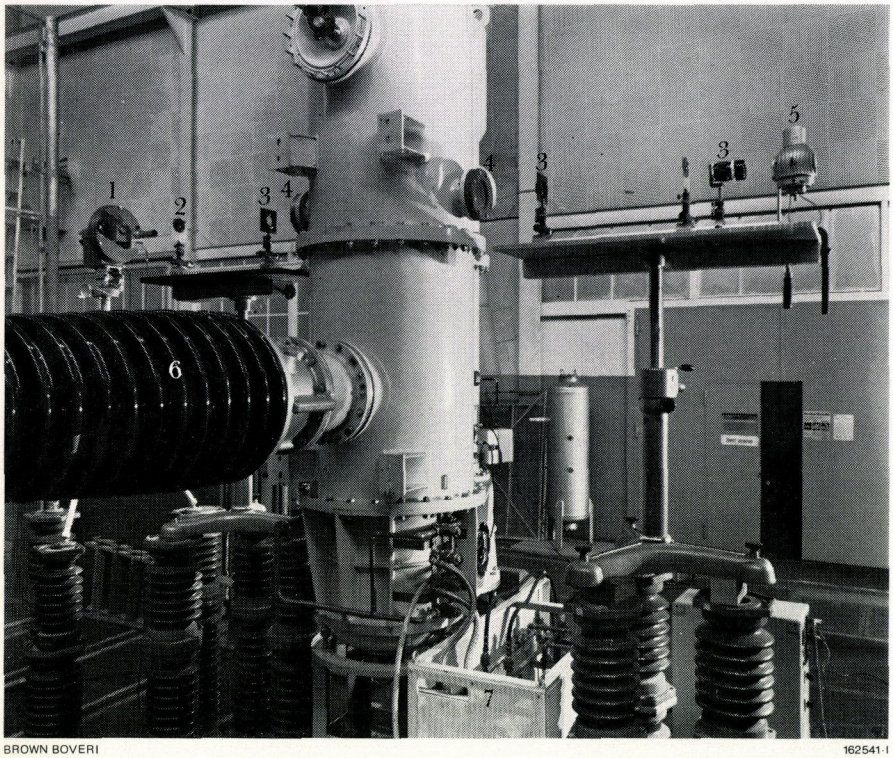

BROWN BOVERI 162541 I

Fig. 4 – Schlieren apparatus on a type ECK differential-pressure SF_6 circuit-breaker

1 = Dynafax camera
2 = Schlieren diaphragm
3 = Lens
4 = Window in breaker enclosure
5 = High-pressure mercury lamp
6 = Bushing
7 = Gas supply

intense light of the arc itself is a serious hindrance with this sensitive method, and so a laser is used as the background light source. This emits its whole intensity at one wavelength, and therefore the light of the plasma can be suppressed with a narrow-band interference filter. A high-pressure mercury lamp is sufficient for studying the gas flow when there is no arc.

A schlieren photography set-up can be seen in Fig. 4, while Fig. 5 shows eddies in the gas stream between the nozzles of a circuit-breaker. The density at the centre of an eddy is sharply reduced, and when the eddy is in an unfavourable position this can result in dielectric breakdown between the nozzles. Through appropriate design modifications it has been possible to eliminate these eddies and also any tendency towards eddy formation along the nozzle axis (Fig. 5c).

In the past, flow phenomena could be interpreted only by the roundabout way of the relatively costly voltage characteristics method [4]. This technique allowed no more than an indirect assessment of the factors influencing dielectric strength; precise statements on the nature and extent of perturbations in the gas stream were simply not possible. A schlieren picture, on the other hand, yields direct information on the quality of the cold gas flow. The schlieren method provides clear pictorial data from which the effect of design measures on the gas flow can easily be appreciated.

The temperature and density distributions in the immediate vicinity of the arc can also be deduced from quantitative schlieren photographs [5]. Figure 6 shows two schlieren streak pictures in which the fringes on either side of the arc are produced by the background light source and are a

Fig. 5 – Schlieren photographs of flow between nozzles, (a, b) before and (c) after suppression of eddies

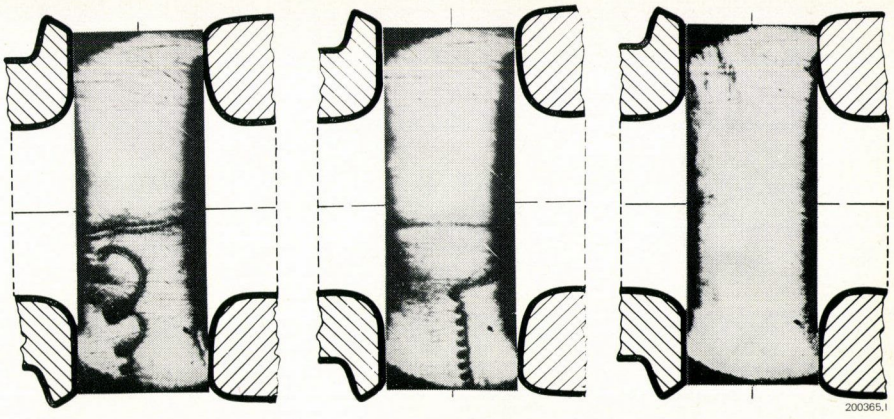

measure of the temperature distribution outside the arc. The comparison between a stable and a pulsating arc shows clearly the influence of the arc on the surrounding gas. These investigations yield particularly interesting findings close to current zero.

The differential interferometer is very useful for locating exactly the maximum density and temperature gradients at the edge of the arc [6]. This method of measurement was originally developed for microscopy and then also employed in the field of gas dynamics for visualizing shock waves. Extreme density gradients are a feature of the strongly blown arcs, and are therefore very well suited for study with differential interferometers. Figure 7 shows the diffraction pattern of a record of this kind. From the displacement of the fringes one can determine the distribution of the refractive index, and hence of the gas density. This method allows extremely accurate measurement of the arc diameter and can also be used as a streak technique for recording the behaviour in time of rapidly changing processes.

Interferometry has for a long time been the most precise, and most difficult, method of visualizing flow phenomena. Through the use of modern lasers (giant-pulse ruby lasers) the experimental complexities of this technique have been reduced to such an extent that it can be employed on a circuit-breaker test rig. The interferogram shown in Fig. 8 was obtained from a double-exposure hologram, one hologram of a switching arc being superimposed on another with no arc [7]. In the original one can distinguish some 170 interference fringes which, when evaluated, provided extremely precise information on the inter-action between the arc and the gas stream. In this

Fig. 6 – Quantitative schlieren streak method of visualizing temperature distribution outside a stable (a) and a pulsating arc (b). The time axis runs from left to right.

D = Diameter of arc

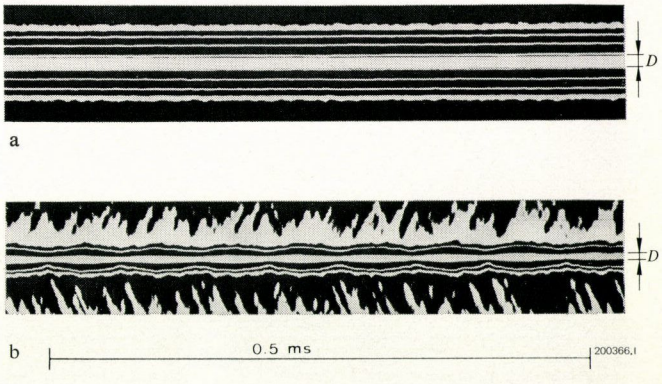

Fig. 7 – Fringe pattern obtained with a differential interferometer

a: Without arc
b: With arc

D = Diameter of arc

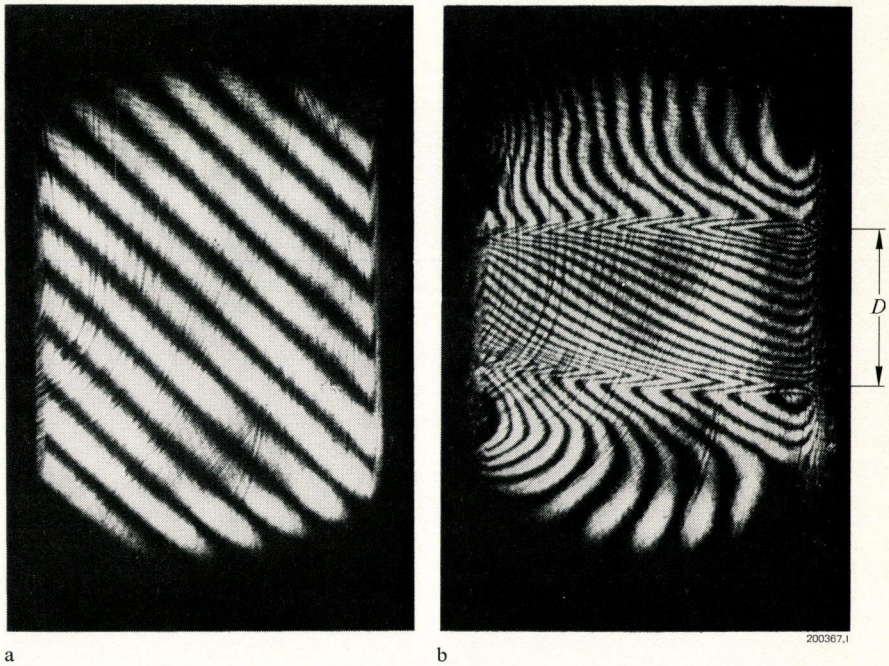

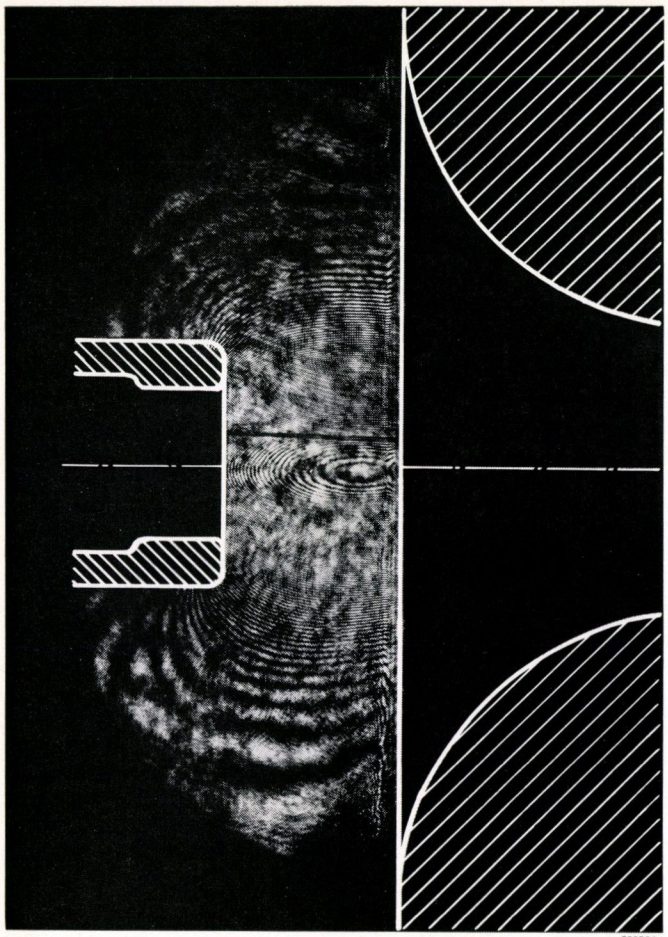

Fig. 8 – Holographic interference pattern of a switching arc

way it was possible to check in detail certain theoretical ideas concerning the major physical processes (such absorption of radiation at the arc boundary). These processes determine the energy transfer from the hot arc to the surrounding gas envelope. Such information is required for deriving theoretical models which are then used in the dimensioning and optimizing of circuit-breakers [2].

Conclusion

Optical measuring techniques have the advantage, apart from those already mentioned, that they in no way influence the arc-quenching process in the circuit-breaker. They help to cut down the enormous cost of testing, and add to our understanding of what happens in the contact region of circuit-breakers. In our high-power testing station, therefore, optical measuring apparatus has become a routine aid in the development of the new ELK puffer-type circuit-breaker.

Another example of the successful application of these optical diagnostic methods is the type tests we have carried out with the ECK type differential-pressure breaker. The oscillograms in Fig. 9 show that today a three-phase breaking capacity of 17 GVA at a voltage rating of 245 kV can be attained with a single extinction chamber per pole.

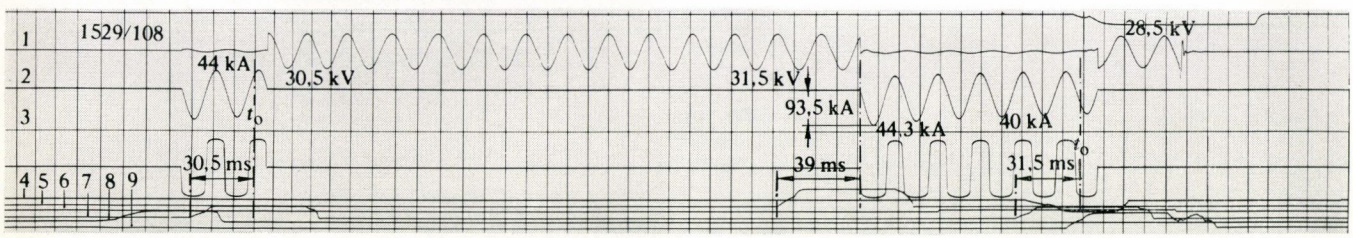

a

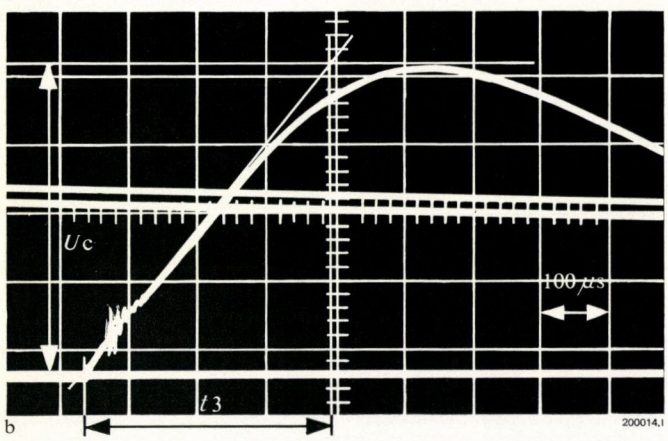

b

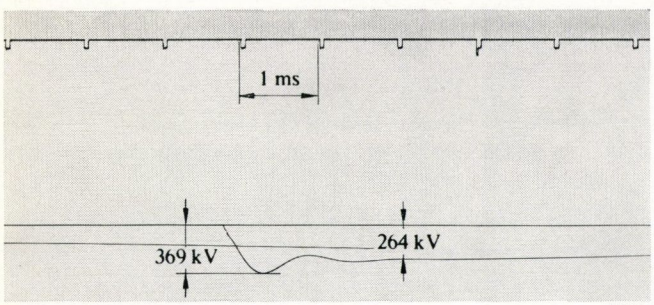

c

Fig. 9 – Oscillograms of autoreclosure in a synthetic test circuit with voltage injection. Complete-pole test of a type ECK differential-pressure SF_6 breaker for 245 kV, with one extinction chamber per pole for a breaking current of 40 kA and first-phase-to-clear factor 1·3

a: Magnetic oscillogram

b, c: Cathode ray oscillograms of recovery voltage across test breaker after second interruption

1 = Voltage in high-current circuit
2, 3 = Short-circuit current (breaking current)
4 to 10 = Commands to test breaker and auxiliary breakers
t_0 = Instant of contact separation in test breaker

	Recommended (IEC)		Measured
Voltage, r.m.s. $\frac{245\text{ kV}}{\sqrt{3}} \times 1{\cdot}3 = 184$		kV	
Voltage, peak (u_c)	365	kV	369 kV
Time coordinate (t_3)	365	µs	365 µs
Rate of rise of recovery voltage $\frac{u_c}{t_3} = 1000$ V/µs			1010 V/µs

Type tests for other switching conditions according to IEC, such as test duties 1, 2 and 3 and out-of-phase switching, conducted mostly in the short-circuit facility of the N.V. tot Keuring van Electrotechnische Materialen (KEMA), have also been successful.
Optical measuring techniques have become a standard diagnostic aid in our testing station. The optical equipment used, particularly in the case of schlieren and streak methods, is rugged and dependable. As a result it is possible to corroborate, and sometimes modify, existing theories on the arc. Armed with the knowledge thus acquired concerning the nature and behaviour of the arc, the circuit-breaker designer can devise extinction chambers of sophisticated design, and convert them into reality.

Bibliography

[1] *A. Mayer, P. Pratl:* Measurement techniques and equipment for testing circuit-breakers. Brown Boveri Rev. *55* 1968 (12) 727–733.

[2] *W. Hermann, R. Horst, K. Ragaller, M. J. Sanders*: Interaction between an electric arc and the flow of gaseous quenching medium. Brown Boveri Rev. *61* 1974 (4) 130–134.

[3] *G. Mauthe, W. Bischofberger, K.-D. Schmidt, A. Ueber:* Type ELK circuit-breakers for metal-enclosed SF_6 insulated switchgear installations. Brown Boveri Rev. *61* 1974 (4) 152–166.

[4] *E. Ruoss:* Test methods and facilities in the high-power testing station. Brown Boveri Rev. *55* 1968 (12) 714–725.

[5] *U. Kogelschatz, W. R. Schneider:* Quantitative schlieren techniques applied to high-current arc investigations. Appl. Optics *11* 1972 (8) 1822–1832.

[6] *U. Kogelschatz:* Application of a simple differential interferometer to high-current arc discharges. Appl. Optics *13* 1974 (8) 1749–1752.

[7] *B. Ineichen, U. Kogelschatz, R. Dändliker:* Schlieren diagnostics and interferometry of an arc discharge using pulsed holography. Appl. Optics *12* 1973 (11) 2554–2556.

Fourth Series of Trolleybuses for Lugano

S. Manzoni

Four two-axle and four articulated trolleybuses have gone into service for the Lugano Transport Authority (Azienda Comunale dei Trasporti di Lugano, ACT). These vehicles have certain features which distinguish them from standard trolleybuses of today. The main reason for these special designs is that the vehicles must travel widely differing routes.

Introduction

The town of Lugano is developing more and more into a centre of business, culture, tourism, administration and education.

In order to cope with the resultant increase in traffic density in the town centre the urban council decided to make public transport services more attractive. ACT recently ordered eight trolleybuses to permit them to increase services and extend them beyond their previous termini. The first vehicle went into service in July 1974. These vehicles have traditional electrical equipment with current control by resistors and electro-pneumatic contactors. The contactors are controlled by an electronic system which replaces the normal cam switches operated direct by the control pedal.

The Lugano Transport System (ACT)

ACT celebrated its 75th anniversary in 1971. Trams were introduced in 1896 and continued operation until 1959. They originally ran on three-phase supply, but, in 1910, when new vehicles were required in order to open further lines, the three-phase system was converted to d.c. For coordination reasons the same voltage, i.e. 1000 V, was selected as for the two local narrow-gauge railway systems between Lugano and Tesserete and Lugano, Cadro and Dino, although this was an exceptionally high voltage for an urban tramway.

Between 1954 and 1959 the tramway services were gradually replaced by trolleybuses supplied from the existing substations. Seventeen trolleybuses (Nos. 101 to 117) were in operation by 1971.

By far the greatest increase in traffic in the town over the last 30 years stems from the private motor car. The

Fig. 1 – One of the fourth series of articulated trolleybuses for Lugano

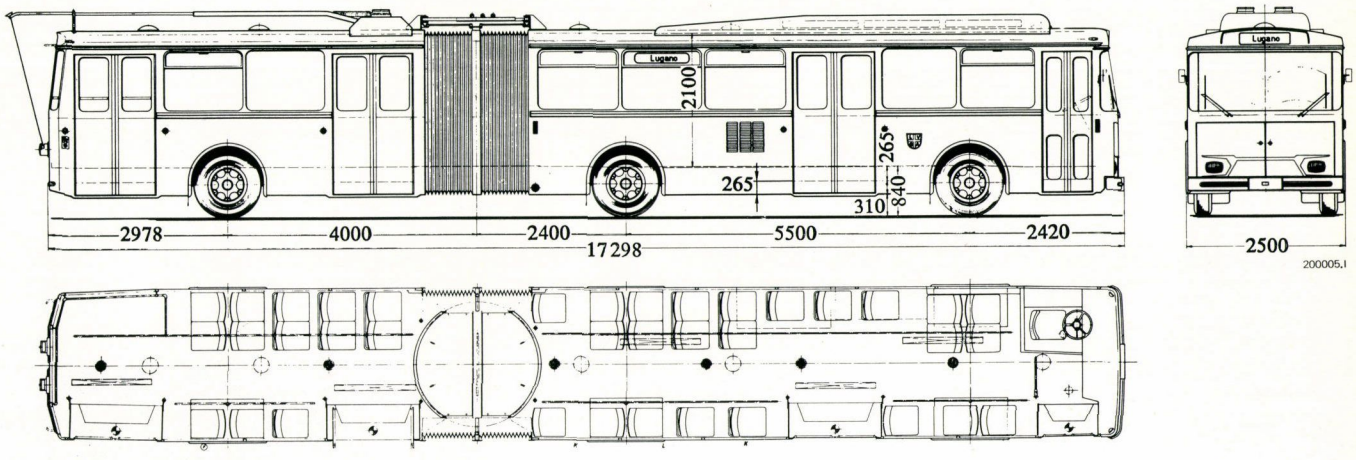

Fig. 2 – Articulated trolleybus

Fig. 3 – Two-axle trolleybus

1 = Traction motor
2 = Inductive shunt
3 = Contactor bank
4 = 1000 V equipment unit
5 = 24 V control panel
6 = Electronic control equipment
7 = Motor/compressor/generator set
8 = Battery
9 = Socket for charging battery

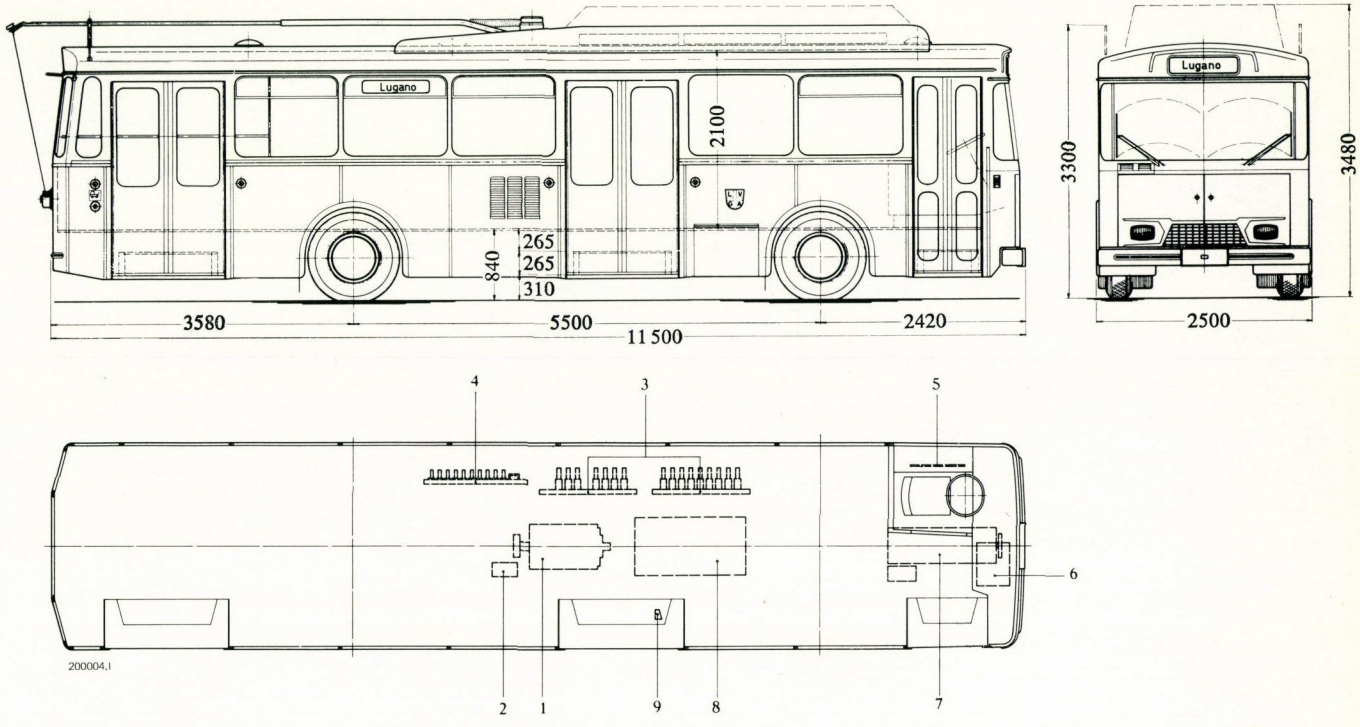

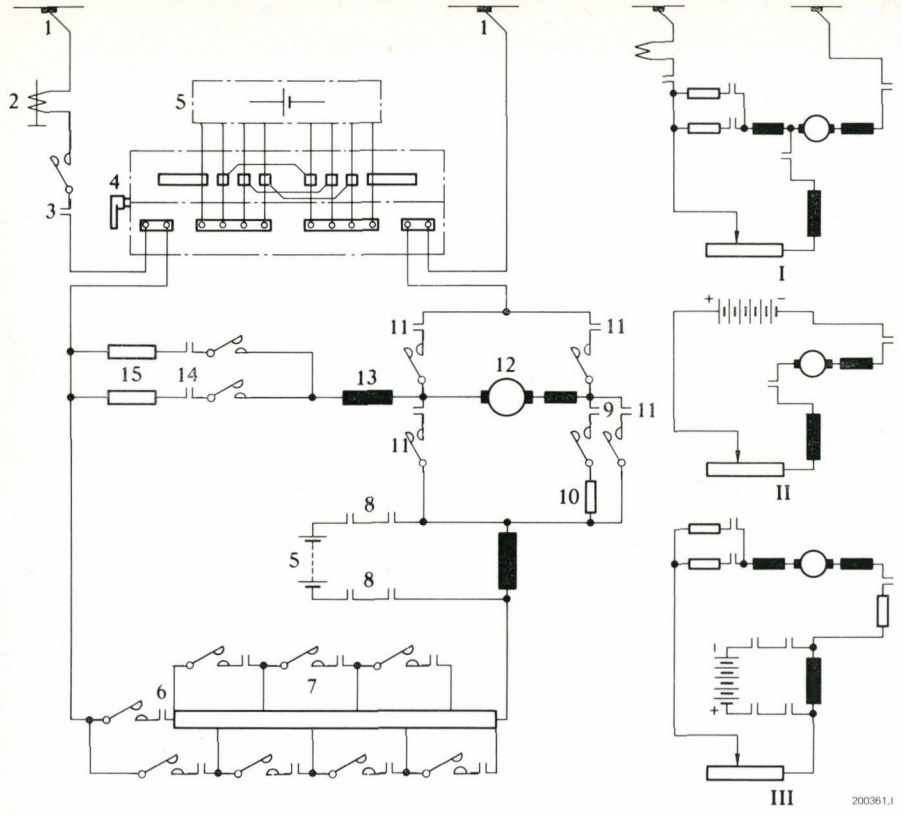

Fig. 4 – Main current circuit
1 = Current collector
2 = Overcurrent relay
3 = Line contactor
4 = Contact wire/battery changeover switch
5 = Battery
6 = Contactors
7 = Starting and braking resistors
8 = Motor pre-excitation contactor
9 = Braking contactor
10 = Additional braking resistor
11 = Reversing contactors
12 = Traction motor
13 = Inductive shunt
14 = Shunt contactors
15 = Shunt resistor
I = Current circuit for motoring with supply from contact wires
II = Current circuit for motoring with supply from battery
III = Current circuit for braking

resultant traffic jams made the local authorities tackle this difficult problem. The decisions arrived at in respect of more rational utilization of available road surface included increasing the capacity of the public transport system. A loan was approved to enable ACT to aquire 11 buses and 8 trolleybuses, of which 4 are two-axle vehicles and the others articulated (Fig. 1).

Design and Construction

Firms involved in building the trolleybuses (Fig. 2 and 3) include:

Chassis:	Automobiles Volvo S.A., Lyss
Bodies, pivots and chassis for the Schenk semi-trailers:	Carrosserie Hess AG, Bellach
Electrical equipment:	S.A. des Ateliers de Sécheron

The Volvo B 58 chassis is derived from a bus frame built in regular production in Gothenburg. The pneumatic suspension for the front and rear axles is supported by leaf springs. The Volvo 1841 rear axle is used mainly for heavy goods vehicles and has simple hypoid gearing with reduction gears in the wheel hubs. The traction motor is connected to the differential gearing through an isolating coupling and cardan shaft. The trailer wheels also steer.
The body is all aluminium. The passenger compartment is bolted to the chassis forming a rigid unit. The skeleton is an all-welded structure of Unidal alloy welded according to the MIG system. The front roof panel and all four roof corners are glass fibre reinforced polyester mouldings. The air inlet for cooling the traction motor is in the right-hand side wall of the vehicle about 1·5 m above ground. With the object of rationalization, both two-axle and articulated vehicles are fitted with the same electrical equipment in identical arrangements.
The two-axle vehicles have a power reserve which permits them to pull a trailer if required. There are only two pedals, both to the right of the steering column. The brake pedal increases the electrical braking effort when depressed and reaches maximum effort at about half travel. Increasing the travel operates the air brakes in proportion to the amount of depression.

Main Data of Vehicles

Mechanical

Tyres	11·00 × 20
Wheel diameter [mm]	1020
Transmission ratio	9·76:1

	2-axle bus	Articulated bus
Weight of mechanical equipment [t]	7·9	11·7
Weight of electrical equipment [t]	2·9	2·9
Total unladen weight (tare) [t]	10·8	14·6

No. of passengers:	2-axle bus	Articulated bus
– seats	23 + 1	37 + 1
– standing	70	110
Total	100	148

Electrical

Normal contact wire voltage [V]	1000
Voltage range [V]	750 to 1200
No. of motors	1

	Continuous	1-hour	Maximum
Power at drive axle [kW]	134	165	
Tractive effort at wheel rim at 100% excitation [kN]	19	26	53
Speed of traction motor [rev/min]	1260	1115	3040
Speed [km/h]	25	22	60
Traction motor current [A]	145	180	300

Traction Motor Circuit

The traction motor circuit (Fig. 4) includes the following equipment:

– 1 overcurrent relay which opens the line breaker, reversing and isolating contactors in the event of an overcurrent.
– 1 line breaker (PH 12·04) designed for 1200 V rated voltage, 400 A continuous current and a 5 min current of 850 A.
– 1 manual contact wire/battery switch for supplying the traction motor from the contact wire or from the battery. Battery supply is used for shunting the trolleybus in the depot, travelling round temporary diversions and continuing the journey if the contact wire supply should fail. This form of traction requires a relatively high-capacity battery. The battery installed comprises four groups of 70 Ah at 24 V with a discharge period of 10 hours. When motoring off the battery the four groups are connected in series which provides the traction motor with a 96 V supply. With a full load (25·5 t) the trolleybus can travel along the flat at 5 km/h and climb an 8% incline at 1 km/h.
– 8 tapping contactors and two shunt contactors for controlling the vehicle speed, 3 isolating and reversing contactors and 1 contactor for reversing with battery supply. All these contactors are of the same type and are installed in two contactor cubicles on the left-hand side of the vehicle (Fig. 5).
– A range of resistor cubicles, including motoring and braking resistors, shunt resistors and extra braking resistors. These are of corrugated Nichrome wire and are mounted on the roof for slipstream cooling.
– A type 4 ELG 2553a non-compensated, self-cooled, four-pole traction motor with interpole windings for series excitation. The one-hour shaft output is 165 kW at 1115 rev/min (approx. 26 km/h). The maximum torque of 2·845 kN m is constant up to a speed of 915 rev/min (approx. 18 km/h). Maximum speed is 3040 rev/min, corresponding to the maximum speed of 60 km/h.

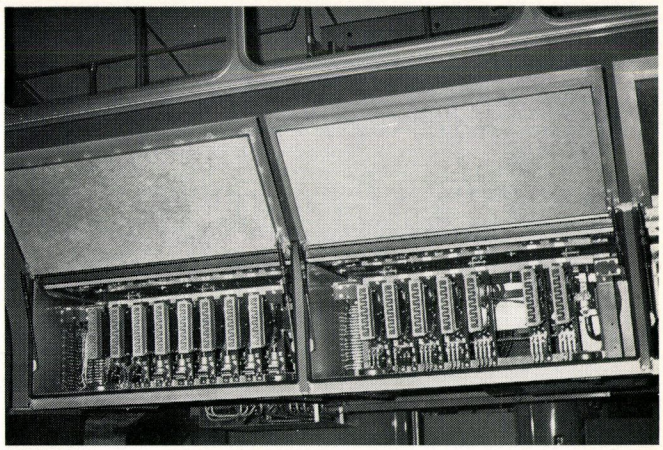

Fig. 5 – Contactor bank

The motors have cast steel casings with nodular cast iron flanges and grease-lubricated ball and roller bearings. The brush gear is mounted direct on the end shields.
The main and interpole coils are insulated to class F and the armature to class H. The individual conductors are insulated with 'Kapton' and the coils with 'Nomex M'. The motor weighs 920 kg.

Fig. 6 – Vehicle characteristics
E = Degree of excitation of traction motor in %
I = Traction motor current
Z = Tractive effort at wheel periphery
c = Duty point for continuous duty
v = Vehicle speed in km/h
1h = Duty point for 1-hour duty
1 to 14 = Tappings at full traction motor field
15 to 17 = Field weakening stages

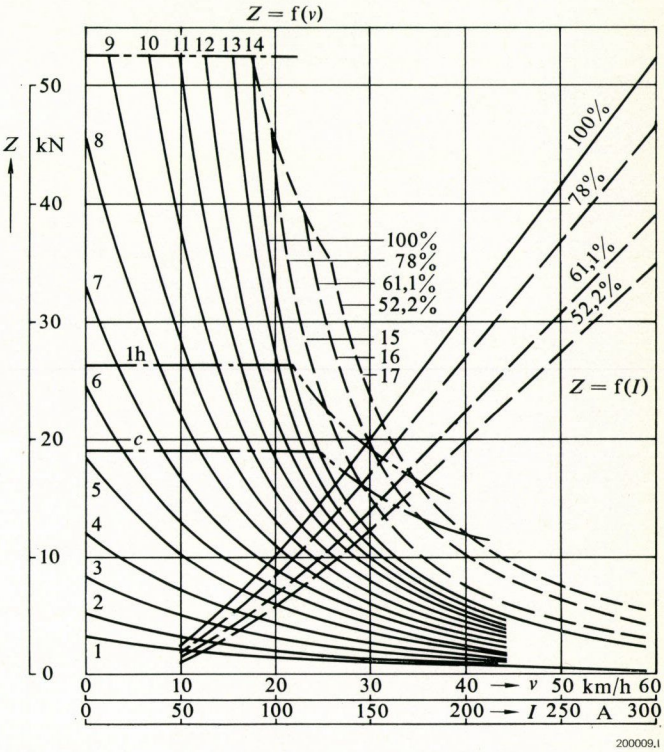

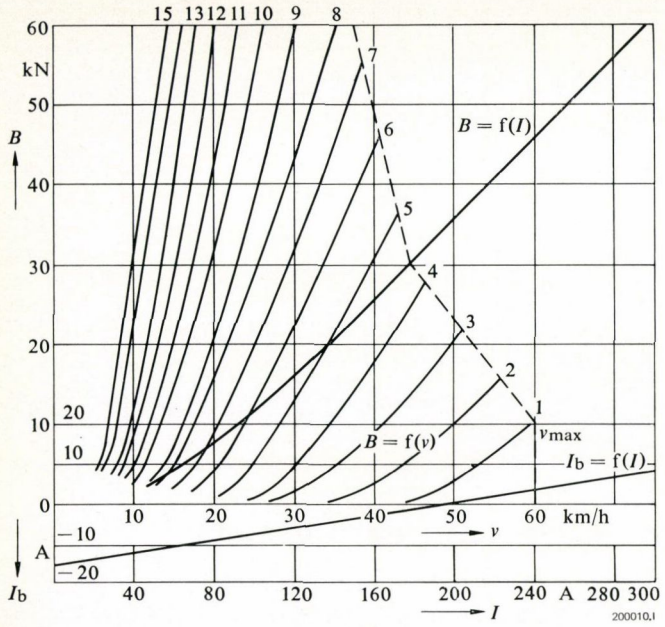

Fig. 7 – Vehicle braking characteristic

B = Braking effort at wheel periphery in kN
I = Motor current in A
I_b = Pre-excitation current in A
v = Vehicle speed in km/h

Performance

Under full load (total 25·5 t) the articulated trolleybus has an acceleration rate of 1·4 m/s² on the flat and 0·7 m/s² on an 8% gradient. As shown in Fig. 6 it can climb a 15% incline with the same loading.
There are 14 acceleration tappings (resistance stages) with an additional three field weakening stages.
Jerk-free electric braking is achieved by pre-exciting the motor from the battery. During electric braking the motor works as a series generator and feeds the power to the starting resistors which are augmented by fixed-value additional braking resistors. Electric braking reduces the speed to about 10 km/h (Fig. 7). The trailer wheels are braked pneumatically while the trolleybus is braking electrically. The pressure in the braking cylinder is proportional to the braking effort of the electrical brakes and the loading of the trailer.

Auxiliaries

Auxiliaries fed from the contact wire include:

– 1 machine set comprising motor, compressor and a.c. generator. The motor is a compound motor of approx. 6·5 kW at 1500 rev/min, the compressor has a throughput of 400 l/min and the a.c. generator has a maximum output of 1·7 kW. One end of the motor shaft drives the generator and the other drives the compressor through a pneumatically operated friction clutch. The compressor clutch is engaged if the pressure in the pneumatic circuit drops below 6·5 bar. When the pressure reaches 8·5 bar the clutch is disengaged. The compressor supplies the air brakes, the pneumatic suspension, door operating mechanism and pneumatic contactors.
– Heating elements with a total output of 8·5 kW with natural convection in the two-axle trolleybus and 13·2 kW in the articulated vehicles. The heating has three control positions; $^1/_3$, $^2/_3$ and full output. The heating elements are distributed evenly along the sides of the vehicles.
– The defroster has a separate fan and a maximum output of 6 kW with 3 control positions.

Electronic Control

Starting, motoring and electric braking is controlled by electronic equipment. The driver's commands are converted into switching commands for the tapping and field weakening contactors. This greatly simplifies the driver's job. At the same time passenger comfort is increased and effective protection is afforded the traction motor. The equipment permits:

– Starting with automatically controlled acceleration for any loading of the vehicle and road incline. The motor is stressed to its loading limit but cannot be overloaded.
– Electric braking at a rate of retardation which is independent of load and gradient, provided that the loading limit of the motor and the maximum permissible commutator voltage is not exceeded.
– Jerk-free reapplication of tractive effort or braking effort of the electric brakes.
– Various other functions such as limiting the jerk-rate, automatic notch-down of tappings if the maximum permissible speed is exceeded, blocking pre-excitation if the vehicle speed drops below 3 km/h and control of the air brakes on the trailer.

The electronic control equipment is at the front of the vehicle and is in the form of a standard rack (Fig. 8) containing 13 modules specially designed for traction applications (Fig. 9). The modules comprise diecast aluminium frames with printed circuits mounted on them. The modules have an interlock. The plug-in connections of each frame have gold-plated contacts. Each unit has its own socket. The specific functions of each module are finite. The 13th unit is a check module and is used for performing functional checks on the other 12 modules at the depot.
The principle of the electronic control equipment (Fig. 10) can be represented diagrammatically as follows:

The position of the motoring/braking pedal determines the required acceleration a_0 and the motoring or braking stage U_{c0} which must not be exceeded.
The tachogenerator driven by the traction motor supplies a signal which is proportional to the vehicle speed v. The first derivative of the speed provides the vehicle acceleration a and the second derivative is the change in acceleration or jerk rate. A d.c. transformer supplies a signal I which is proportional to the motor current. The desired acceleration a_0 is compared with the actual acceleration a and the permissible motor current, jerk rate and maximum permissible speed are taken into account.
During braking the desired retardation a_0 is compared with the actual deceleration a taking the permissible commutator voltage into account.
Pre-excitation by the battery comes into effect only at speeds greater than 3 km/h.
The signals 'motoring' and 'braking' pass through changeover switches and reach a gate which permits only the

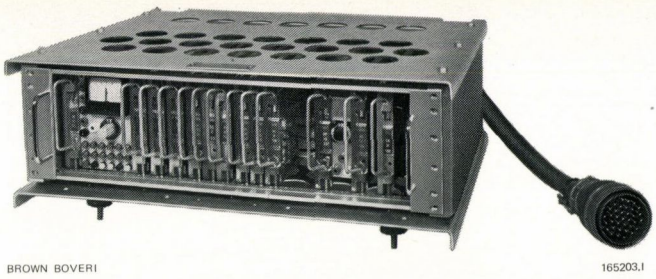

Fig. 8 – Electronic control rack

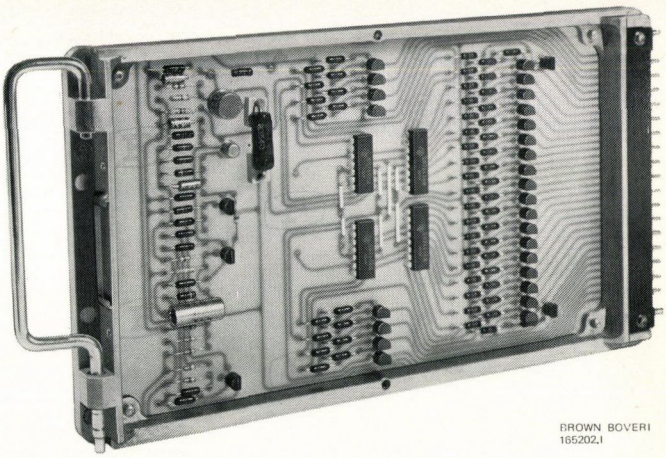

Fig. 9 – Plug-in module

largest signal to pass. The changeover switches check whether the grouping contactors are in the correct position for motoring or braking. If, for any reason, the main current connection is not correct, the controller prevents notching up or instigates automatic notch down.

The signal from the gate passes to an integrator which supplies the control voltage U_c. This is controlled by a level limiter and a pulse generator for notching up to U_{c0}, or the limiter blocks notching, depending on whether the circuit is correct or not. The pulse generator for notching up permits much more rapid notching when braking is instigated, up to a level which is a function of vehicle speed v and the desired acceleration a_0. The signal for rapid notching up passes through a changeover switch controlled by a gate. The gate checks whether the main current circuit for braking is live and whether the motor current is less than 40 A. The voltage U_c, whose value corresponds to a certain degree to the angular position of the classic cam switch operated by the pedals, controls switching of the tapping and shunt contactors through trip units which activate the contactor valves. Each trip unit becomes conducting, i.e. it switches on, when the voltage U_c exceeds the reference voltage for the corresponding trip unit. By the same token the trip unit switches off when U_c drops below the reference voltage. The value of voltage U_c determines the motoring stage and the value of its derivative determines the cadence of notching up or down. A switching programme can be compiled by arranging the reference voltages of the trip units in stages (e.g. in 5 V steps).

Double Insulation

In the case of most electric rail traction systems the vehicles and the return current conductors are connected to earth. There can therefore be no voltage difference between the vehicles and earth.

In the case of trolleybuses the body and chassis are insulated from earth by the tyres and by the contact

Fig. 10 – Function diagram of the electronic control system

1 = Motoring/braking pedal
2 = Variable capacitor
3 = Desired acceleration
4 = Maximum notch
5 = Tachogenerator
6 = Differentiator
7 = Transducer
8 = Current limiting
9 = Jerk rate
10 = Maximum speed
11 = Voltage limiting during braking
12 = Pre-excitation
13 = Motoring circuit
14 = Braking circuit
15 = Motoring changeover switch
16 = Braking changeover switch
17 = Notch-down
18 = Maximum value transmitter
19 = Integrator
20 = Level limiting
21 = Level changeover
22 = Rapid notching
23 = Braking stage
24 = Changeover
25 = Gate
26 = Motoring/braking
27 = Output stages
28 = Solenoid contactor coils

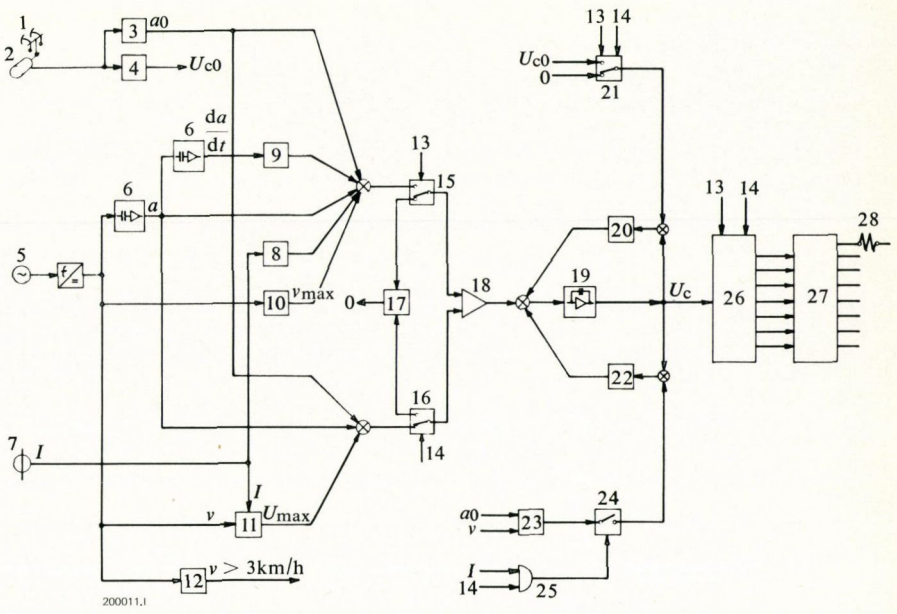

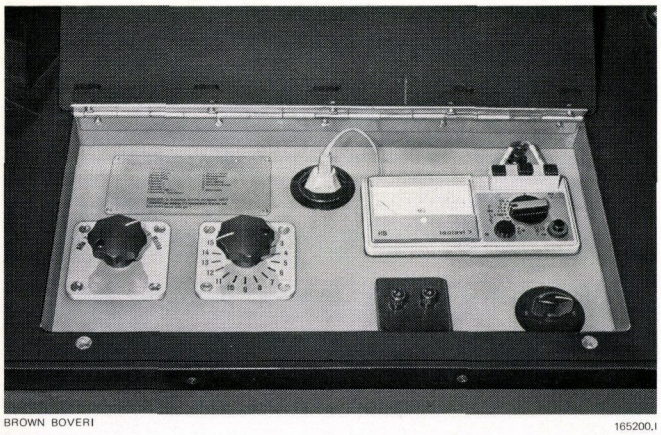

Fig. 11 – Insulation check and measuring unit

wire conductors. One of the two conductors is normally earthed at the substation. A fault in the insulation of the electrical equipment can cause such a high voltage difference between the vehicle and earth that a passenger about to enter the vehicle and touching a metal part of the trolleybus could sustain an electric shock which could be unpleasant or even dangerous.

Passenger safety therefore requires double insulation of all high-voltage equipment and a test system for both insulations. The insulation check equipment (Fig. 11) comprises an ohmmeter, a changeover switch and selector switch. The latter enables that piece of equipment which is to be tested, to be selected. The changeover switch permits either of the two insulations of that piece of equipment to be selected.

It is also possible to carry out an insulation check on the various equipment by using a voltage supply of several kV at 50 Hz in place of the ohmmeter.

Rectifier Substations for Railways

P. Salzgeber

The author describes the layout of a rectifier substation, discusses aspects of protection gear and protection coordination, and finally touches on an in-house computer programme for optimizing design.

Introduction

Stationary power supply installations are employed mainly for d.c. traction systems such as trams, trolleybuses, standard-gauge railways and underground railways.
The d.c. voltages used for trams and trolleybuses are generally between 500 V and 1000 V, for standard-gauge systems from 1500 V to 3000 V, and for underground railways usually between 600 V and 800 V, with recently 1500 V as well.
Currents are from a few hundred to some thousands of amps; peak currents of some 10 000 A occur in underground systems.
The largest installations today and in the immediate future are for underground railways. Public attention in many cities is at present focussed on the construction or extension of this kind of transport system.
Comparing the various means of urban transport (Table) shows quite clearly the advantages of tram, underground and rapid transit railway over other forms of traffic. A further significant advantage of these three rail systems is relative freedom from pollution.

Layout of Rectifier Substation

The general arrangement of a modern rectifier substation is shown schematically in Fig. 1. The section for the *incoming a.c. power supply,* which usually arrives via overhead lines or cables at 5 to 50 kV, comprises a medium-voltage switching station with isolator, circuit-breaker, lightning arrester and instrument transformer. This is a perfectly conventional medium-voltage installation and need not be described further here.
Particularly in the case of underground railways it is best to provide a medium-voltage ring main to allow internal transfer of power. For reasons of dependability there should be two separate sources of supply.
The *rectifier transformer* is nowadays usually an oil or pyralene-filled transformer with natural air cooling, designed for the overloads imposed by the rectifier. It is likely that moulded-resin transformers will come to be used more widely in future, firstly because of their high short-time overload capacity, and secondly, especially for installations below ground, because no oil is needed.
The *rectifiers* used are exclusively silicon power diodes in 6 or 12-pulse bridge connection for new plant, or in mid-point connection if replacing mercury-arc rectifiers. The rectifiers are mostly designed for natural air cooling, and so require no maintenance. Moreover, with the usually brief overloads occurring in traction applications the savings achieved with parallel diodes owing to more intensive cooling are in practise cancelled out by the extra cost of fans and supervision.
Design with respect to current is generally in accordance with precisely defined overload classes, such as class V or VI of IEC Publication No. 146, or NEMA Standard RI 9 for very heavy traction [1, 3].
The unit rating of a rectifier ranges from about 1000 to 4000 kW, each substation often containing a number of rectifiers.
The silicon diodes employed have nominal currents of 400 to 500 A. They are obtainable as conventional flat-base

Comparison of urban transport facilities

Facility	Carrying capacity of one 3 m lane Persons/hour	Average speed km/h
Private car	1500	20 to 40
Motorcycle	2400	20 to 40
Bicycle	5400	20
Bus	10 000	15 to 25
Pedestrian	16 000	5
Train	20 000	15 to 25
Underground	25 000 to 40 000	25 to 40
Rapid transit railway	40 000 to 80 000	30 to 60

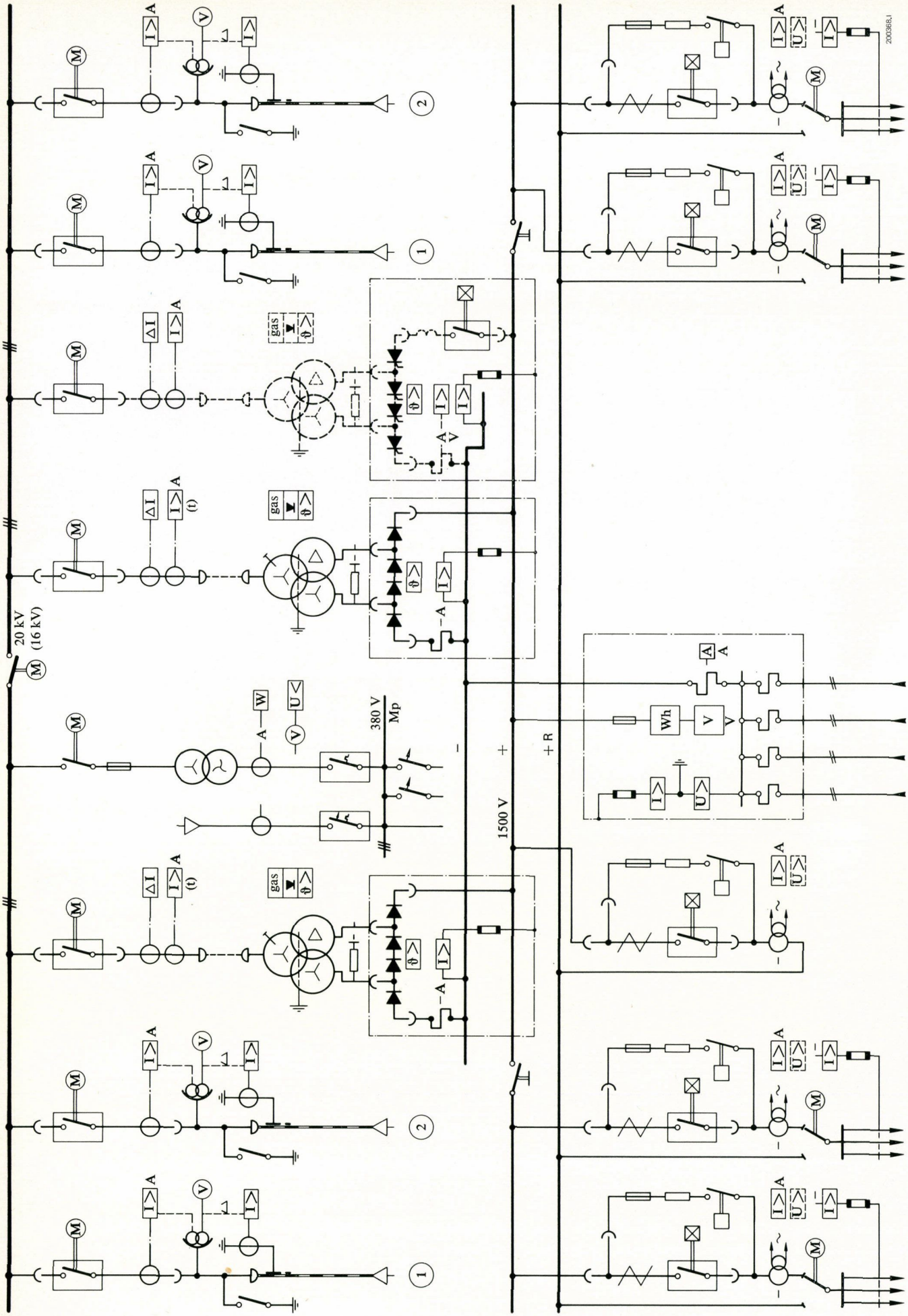

Fig. 1 – Basic circuit of a rectifier substation

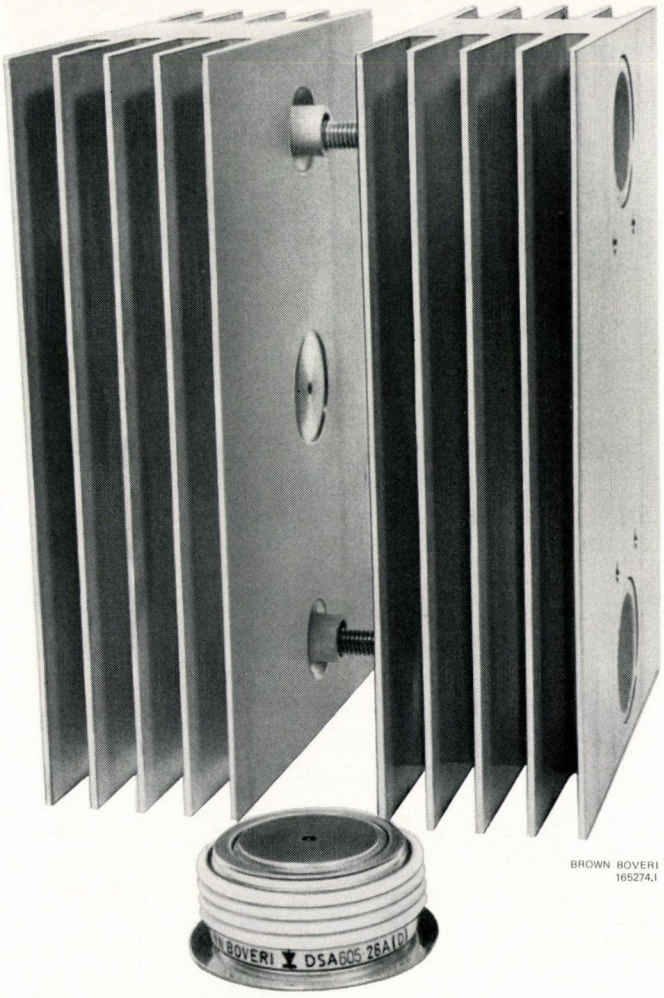

Fig. 2 – DSA 605–26 silicon diode with twin heat sink HN 2

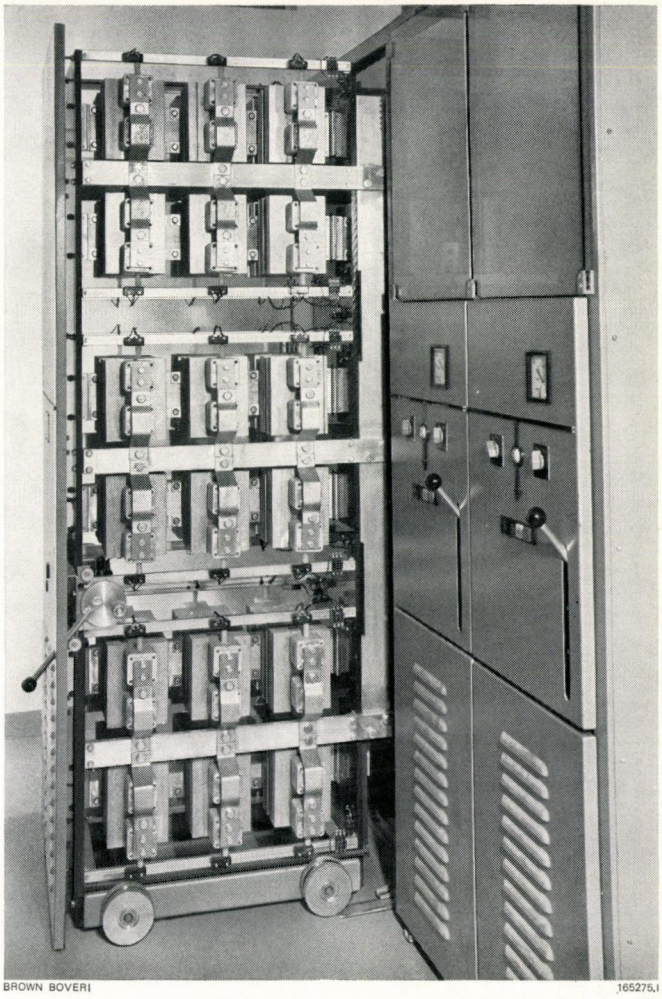

Fig. 3 – Truck-mounted silicon rectifier for 2000 kW/750 V
Overload capacity to IEC class VI: 150 % 2 h, 300 % 1 min

diodes for single-sided cooling with braided lead, or recently as disc-type diodes which are mounted between two heat sinks and provide better dissipation of heat losses.

A silicon power diode of type DSA 605–26 is shown together with its HN 2 twin heat sink in Fig. 2.

The diode assemblies (diode plus heat sink) can be mounted direct on the a.c. busbars of the rectifier since these, together with the two insulating walls, form the supporting frame. This form of construction with no flexible connections results in an easily assembled, clearly arranged layout with a high insulation level. Both fixed and truck-mounted rectifiers are built. The draw-out type requires considerably less space since it need be accessible only from the narrow side.

Figure 3 shows a truck-mounted silicon rectifier of 2000 kW/750 V. Permissible overload to IEC class VI: 150 % 2 h, 300 % 1 min.

With the high blocking-capacity power diodes available today (up to 5000 V) it is possible to build rectifiers for more than 1500 V with only one diode in series. Owing to the avalanche characteristic of these diodes, which are produces by diffusion techniques, overvoltage protection is also much simpler.

As the rectifiers are usually fitted with diode fuses, they are often connected to the d.c. busbars only by way of isolators (motor-driven in remote-controlled stations) and with no cathode switch. All rectifier groups of a substation (two groups are shown in Fig. 1) operate in parallel on a common d.c. bus. The position bar is often supplemented by an auxiliary or bypass bus. In this way any feeder breaker can be bypassed by means of the reserve breaker and auxiliary bus for maintenance purposes.

The outgoing *feeder-breaker* is, next to the rectifier group, probably the most vital item in a substation. Its function is to isolate overloads and short circuits occurring on the line.

Brown Boveri and Sécheron manufacture two types of feeder breaker: the UR 25 high-speed d.c. breaker and the GB semi-high-speed breaker.

The distinctive feature of a high-speed breaker is its short mechanical operating time of less than 3 ms from the moment the tripping value is reached until the contacts open. It is thus possible to limit the short-circuit current while it is still rising. For this reason it is called a current-limiting breaker.

The mechanical response time of the semi-high-speed d.c. breaker, on the other hand, is some ten times longer. The current is therefore interrupted after it has attained the steady-state value. Consequently the amplitude of the current is not limited in any way. But even here the time saving compared with the response of an a.c. breaker is very considerable.

The choice between the two d.c. breakers is very closely

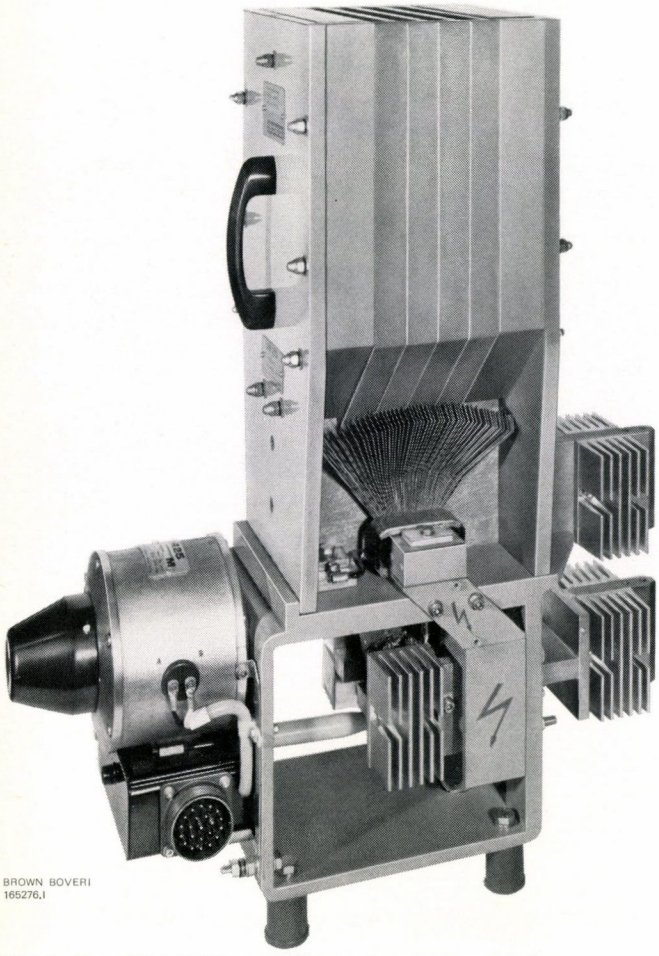

Fig. 4 – Type UR 25 high-speed d.c. circuit-breaker

Fig. 5 – Feeder-breaker cells with draw-out d.c. circuit-breaker type GB

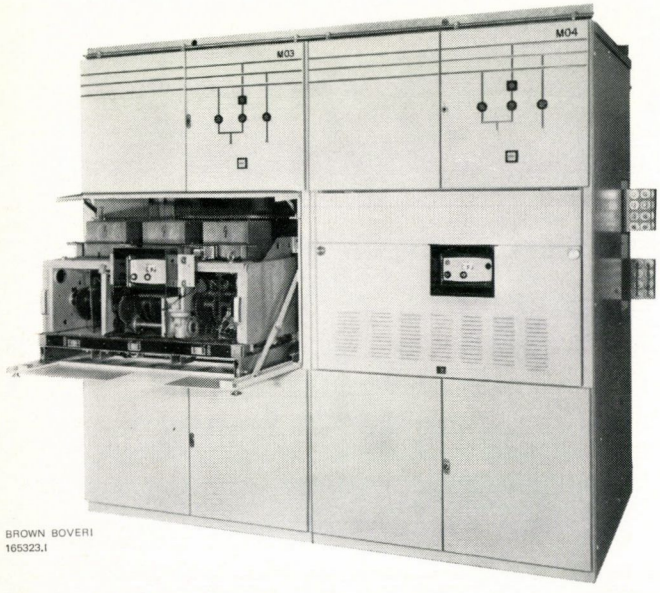

related to the general protection arrangements, which are considered in the following section.

Figure 4 shows a type UR 25 high-speed d.c. breaker such as is used for tram and trolleybus networks and standard-gauge railways up to 2000 V. The new UR 26–40 breaker, for 3000 V, was also developed from this type.

Owing to the ever increasing unit ratings of traction vehicles and the short times between trains, particularly in the case of underground systems, feeder breakers are required to have ever higher rated currents and breaking capacities. A new d.c. circuit-breaker to meet present-day requirements is being developed at Sécheron.

Feeder are usually truck-mounted and housed in cells similar to those for a.c. breakers. The draw-out breaker with an interlocked isolating position eliminates the need for an extra isolator and simplifies servicing and maintenance.

All the breaker control gear, together with the additional protection facilities such as a line tester and perhaps a line fault detector, is contained inside the breaker cell (if possible on the truck).

A breaker cell with a truck-mounted d.c. circuit-breaker type GB can be seen in Fig. 5.

Fig. 6 shows part of a substation with a draw-out rectifier and truck-mounted UR 25 d.c. breakers.

The supplies of auxiliary and control voltage constitute a small, but vital, part of the whole installation and determine its safety and reliability. The a.c. voltage can be drawn from the medium voltage through an auxiliary transformer, or possibly from the local supply system. An auxiliary rectifier maintains a constant charge in the battery which feeds the most important control and signalling systems. An inverter, fed from the contact wire, or a diesel generator set can be provided, depending on the importance of the equipment to be supplied.

Large installations need centralized supervision. This means that remote control facilities are required, and systems for remote measurement of the essential quantities. Modern substations can thus incorporate a fully-fledged telecontrol system.

Protection Gear and Coordination

Protection coordination must cover protection of both personnel and equipment. It is most important that a coordinated protection scheme extending from the vehicle to the incoming a.c. supply should be worked out during the planning of an installation.

A broad distinction can be drawn between three kinds of protection: overcurrent and short-circuit protection, earth-fault protection and overvoltage protection. Overvoltages can be of atmospheric origin or due to switching or commutation process.

Arresters and overvoltage relays are employed on the a.c. side. The rectifier itself is usually protected from external overvoltages by an *RC* network. With avalanche diodes the surge-absorption arrangements are greatly simplified, or dispensed with altogether. The d.c. distribution system needs no special overvoltage protection. Lightning arresters or overvoltage protectors are fitted on the contact wire or third rail. The vehicle should also be provided with an arrester.

The response levels of the various protective devices must be matched. Also, the insulation level of the system components used must be high enough to ensure the equipment is suitably protected.

For an overcurrent and short-circuit protection system to be effective there must be good selectivity from the vehicle to the transformer breaker. It is essential that a fault current should be interrupted as close as possible to its point or origin. For this reason the vehicles should also be equipped with a high-capacity breaker. Good time grading can be achieved with a high-speed d.c. breaker on the vehicle, a semi-high-speed breaker as the feeder breaker and an a.c. breaker.

The feeder breaker must disconnect overloads on the contact wire or conductor rail. It must also have sufficient breaking capacity to handle the short-circuit power when all the rectifier groups in a station are operating in parallel.

In addition to an actual dead short, distant or relatively high-resistance short circuits can occur on the contact wire or conductor rail, giving rise to currents which are not sufficient to trip a feeder breaker. Short circuits of this kind are particularly dangerous and in the past have caused serious damage because the infeed through the feeder breaker was often not interrupted for some considerable length of time. To remedy this, special line fault detectors (DDL and PCC) have been developed which can distinguish these distant short circuits from normal traction currents, and disconnect them quickly by means of the feeder breaker.

If there is no cathode switch, all short circuits occurring beyond the feeder are interrupted by the transformer breaker. Rectifier and transformer are obviously designed to be short-circuit-proof for the opening time of their a.c. breaker.

An internal diode breakdown is isolated by the appropriate fuse, which also prevents reversed currents from parallel rectifiers.

Particular attention must be paid to earth faults and protection against contact. Two different approaches are adopted towards the installation of rectifiers and switchgear cubicles: the low-resistance technique with earth-fault supervision prevents the cubicles from becoming hot, but allows an arc, i.e. between positive bus and cubicle panel. The high-resistance method, on the other hand, eliminates arcing, but the cubicles can become live.

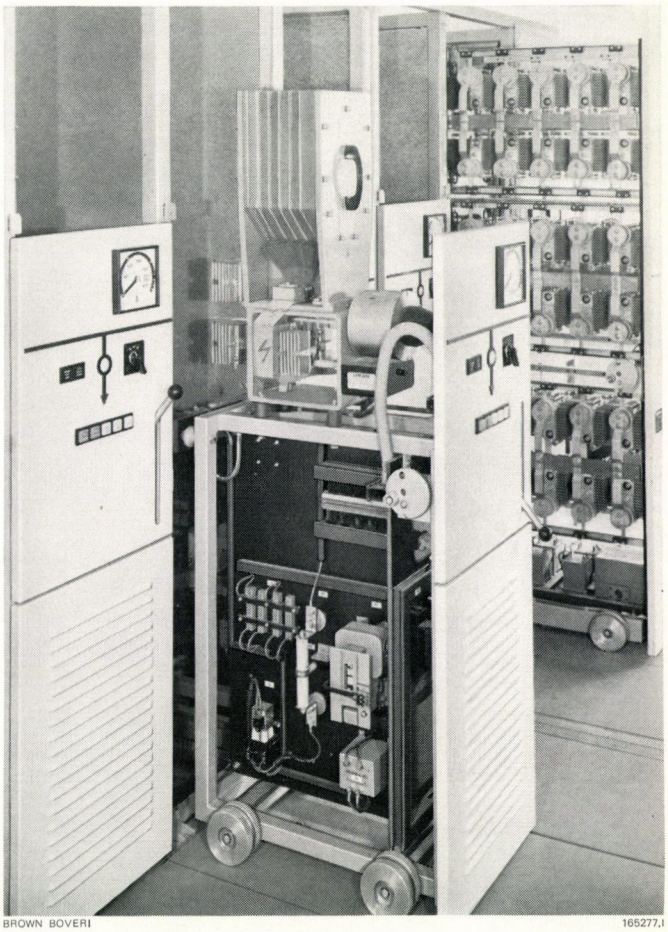

Fig. 6 – Truck-mounted rectifier and type UR 25 d.c. circuit-breaker

It is not really possible to stipulate one single, unified philosophy as account must always be taken of national standards and regulations, and also of specific requirements.

Rectifier and Inverter Operation

The energy present when a train is braked must somehow be dispersed or reutilized. On underground railways the classical method of rheostatic braking can raise the tunnel temperature appreciably.

Regenerative braking presents the possibility of reusing the energy. The braking current is fed back into the d.c. system by the traction motor which functions as a generator. This energy is then drawn by trains running in the vicinity at the time. It can happen, however, that there are no trains sufficiently near, or that several trains brake simultaneously.

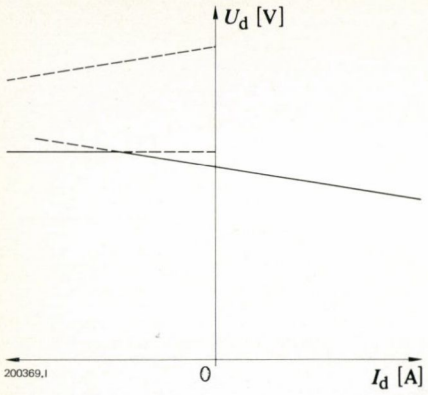

Fig. 7 – Characteristics of rectifier (right) and inverter (left)

To cope with this situation, certain rectifier stations are equipped with an inverter, which allows power to be fed back into the a.c. network. This inverter (shown as broken lines in Fig. 1) is connected to the d.c. bus in parallel with the rectifiers, and begins to feed into the a.c. system the moment the d.c. voltage on the busbar rises above the no-load voltage of the rectifiers.

The inverter is basically of the same construction as the rectifiers, except that controlled thyristors are used instead of diodes. A choke and a high-speed d.c. breaker limit and interrupt the short-circuit current in the event of punch-through.

In Fig. 7 a rectifier characteristic is shown on the right and an inverter characteristic on the left, the voltage being limited by the control electronics. Through compounding it is possible to keep the voltage on the contact wire and at the vehicle within acceptable limits, even with relatively high regeneration currents. The inverter must be designed so that the braking currents can be absorbed without excessively high voltages occurring at the traction motor.

Close cooperation between the builder of the vehicle and the substation supplier is essential in arriving at an inverter of the correct performance.

A Modern Aid to Optimum Design

A programme available in the Brown Boveri computer centre serves as a useful aid in the planning of large installations.

With the computer it is possible to calculate and compare a whole series of variants. Both different configurations of the stationary equipment and various timetable arrangements can be taken into consideration.

The version most favourable from the technical and operational standpoints is selected from the various possibilities with an eye to a reasonable financial outlay.

Optimization of this kind is possible only with the aid of a computer having a substantial storage capacity.

Besides normal operating conditions, one can also simulate disturbances, e.g. due to failure of a substation, and determine their consequences.

The most important input data are: vehicle characteristics, section profile, train frequency and the technical data of the substations.

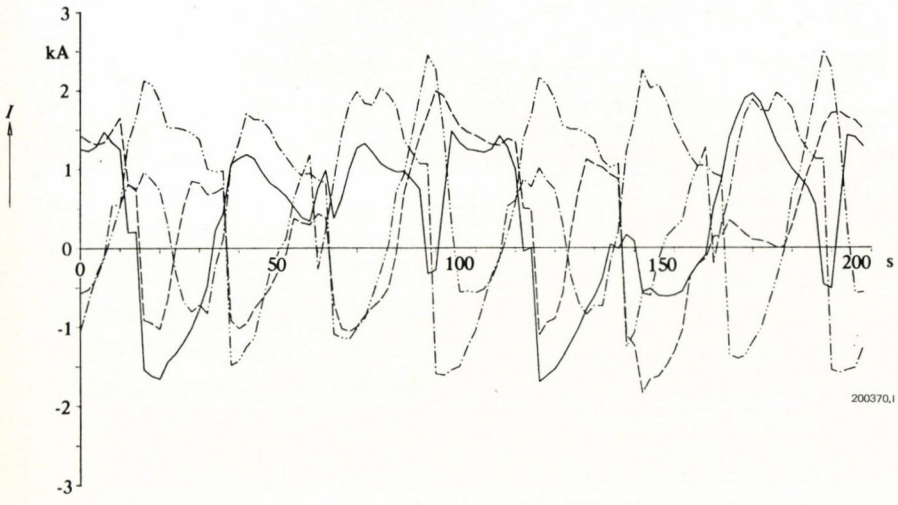

Fig. 8 – Feeder currents I of a substation with four feeders

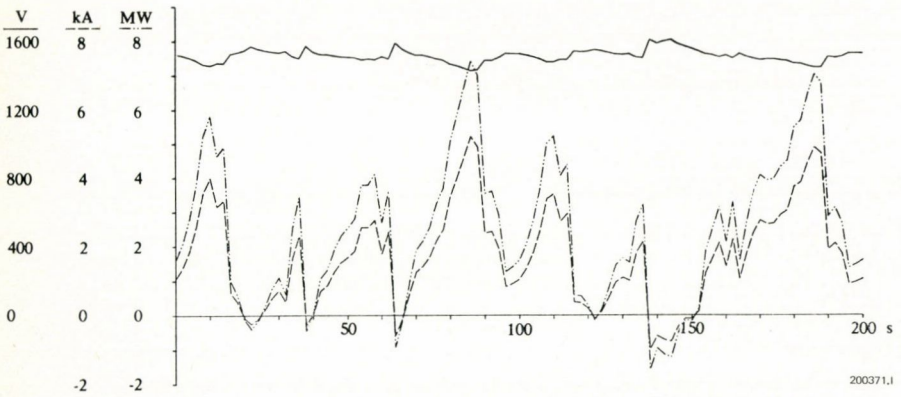

Fig. 9 – Current, voltage and power of a substation

The results, obtained in tabulated or graphical form, provide information on: location and speed of trains, voltage at contact wire, current and power consumption of the vehicles, currents, voltage, power and energy of the substations in rectifier and inverter operation.
All these data make it easier to define the power rating and short-time overload capacity of an installation, and also its location. By capitalizing the power of regeneration it is possible to determine the benefit to be obtained from the extra cost of an inverter.
As an example of calculation, let us consider the following simplified underground railway: route length 20 km, interval between trains 100 s in the middle portion and 200 s at the ends, 20 stops, stopping time 20 s, max. speed 100 km/h, six substations with two rectifiers rated 2500 kW and one inverter rated 2500 kW and four outgoing feeders.
On the basis of this example, Fig. 8 shows time curves of the four feeder currents of substation No. 3 while Fig. 9 depicts the total current, voltage and power of the same substation.

Conclusion

In order to achieve a unified system concept an overall engineering scheme is worked out by the department for traction substations. The appropriate experts on detailed problems concerning protection, remote control, busbar design, etc. are also called upon, thus ensuring that the best possible solution is found.
Brown Boveri and Sécheron act as main contractors for the engineering and delivery of stationary d.c. supply systems, from the incoming a.c. supply, of whatever voltage, until the direct current is fed to the vehicle, including auxiliary supplies and remote control.

Bibliography

[1] Silizium-Gleichrichter-Handbuch. BBC Brown, Boveri & Co., Ltd., Baden, 1970.

[2] Silizium-Stromrichter-Handbuch. BBC Brown, Boveri & Co., Ltd., Baden, 1971.

[3] *H.-R. Wallertshauser:* Gleichrichterunterstationen mit Siliziumleistungsdioden für Bahnanlagen. Bull. Schweiz. Elektrotech. Ver. *57* 1966 (11) 479–485.

Low-Ripple Power Supply for Magnets

R. Gerber

Providing a controlled, low-ripple power supply for an active magnet load requires a high internal resistance for both d.c. and a.c. These conditions can be attained by using passive filter circuits and semiconductor regulating units. The circuit structure and some control aspects relating to the set requirements are discussed.

Introduction

Brown Boveri supplied 68 power supply systems of various outputs and accuracies, and with a total output of 2 MW (Fig. 1) for the European Nuclear Research Centre (CERN) in Geneva. Their purpose is to supply the pole face windings of the main magnets and the quadrupole and sextupole magnets in the intersecting storage rings (ISR)[1].

The quadrupole and sextupole magnets have conventional power supplies. The virtually constant magnet load requires a power supply which respresents a current source of between d.c. and a few Hertz. In the adjacent frequency range the voltage source characteristics (small internal resistance) are adequate to comply with the required ripple.

However, conditions are rather different for the power supply equipment for the pole face windings discussed in the following. The purpose of pole face windings is to correct the main field. Changes in the main field and in the harmonics of the main supply unit induce voltages at the main windings of a magnet and thus affect the pole face windings. Consequently the magnetic load comprises both passive and active components (induced voltages).

Under these conditions the exceptionally stringent requirements made in respect of current ripple (5×10^{-6} I_{max}) must be complied with. It is obvious therefore that the supply equipment must have a high internal resistance (current source) for this type of load even at high frequencies.

[1] *H. C. Appelo, R. Gerber:* 68 medium power supplies for the ISR. CERN/ISR-Po. 24–1973.

Technical Data and Requirements

– Power rating	39 kW (285 V, 135 A)
– Range of current adjustment	0·1 to 100 % I_{max}
– Accuracy over a period of 6 months	$\frac{\Delta I}{I_{max}} \leqslant 10^{-3}$
– Max. ripple	$\frac{i_{r.m.s.}}{I_{max}} = 3{\cdot}7 \,.\, 10^{-6} \triangleq 0{\cdot}5$ mA
– Max. rate of adjustment	$\frac{di}{dt} = 5$ A/s
– Load resistance	$R_L = 2{\cdot}0\ \Omega$
– Load inductance	$L_L = 1{\cdot}0$ to 10 mH
– Load time constant	$T_L = 5$ ms
– Induced voltages at frequencies of 50 to 600 Hz	$U_i \leqslant 2$ V (r.m.s.)

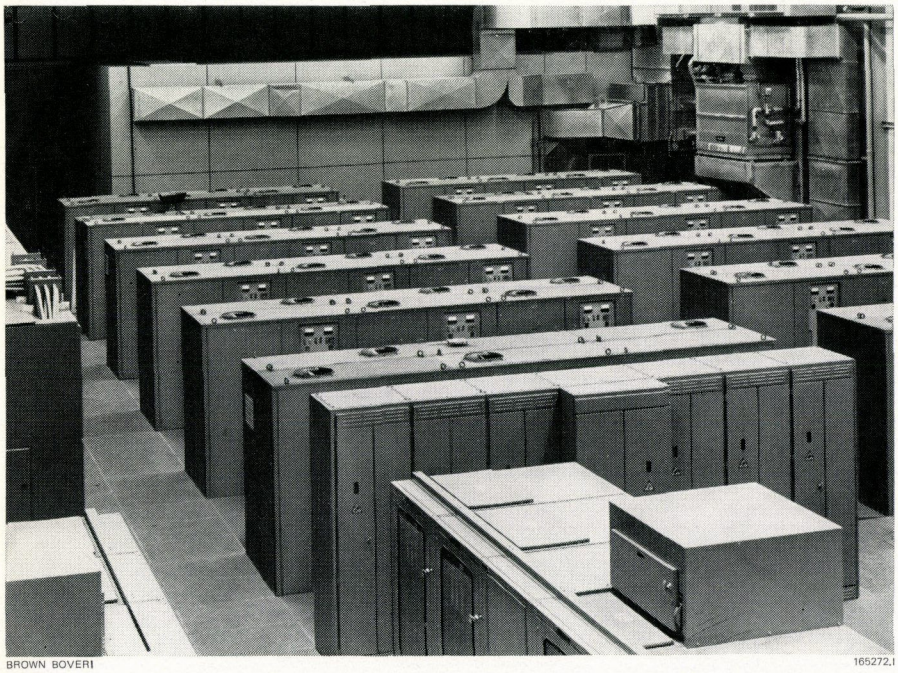

Fig. 1 – View of the power supply equipment for the magnets at the European Nuclear Research Centre in Geneva

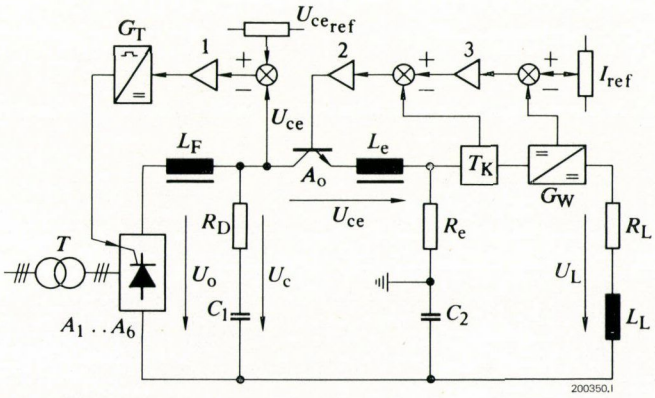

Fig. 2 – Basic circuit diagram for the supply to the main pole face windings

C_2 = Anti-interference capacitor
G_T = Pulse control set
L_L = Load inductance (magnet)
L_e = Emitter choke
R_D = Damping resistor
R_e = Earth resistance
R_L = Magnet resistance
U_c = Voltage at low-pass filter output
U_{ce} = Emitter voltage across transistor
m = Control unit
$U_{ce\,ref}$ = Set point for transistor duty point
U_L = Load voltage (magnet)

Other symbols, see text.

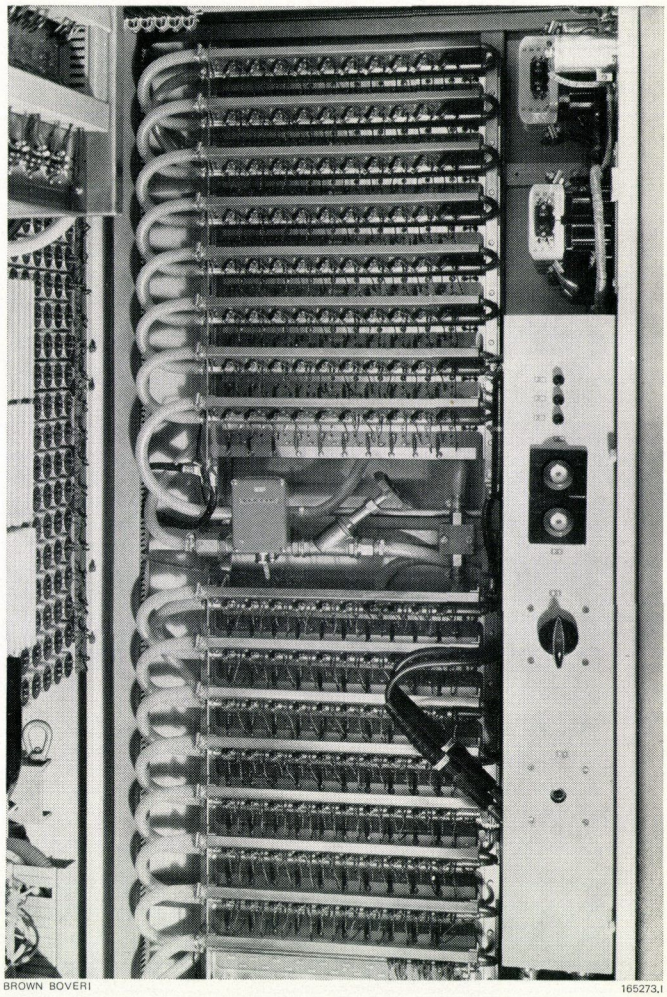

Fig. 3 – Water-cooled transistor control unit comprising 15 units of 10 transistors each

The accuracy of long time stability is guaranteed between d.c. and 10 Hz and must be maintained under the following conditions:

– Gradual changes in supply voltage	90 to 110 % U_n
– Sudden changes in supply voltages	± 5 % U_n
– Frequency range	50 Hz±0·25 Hz
– Temperature range	10 to 40 °C
– Rate of temperature change	4 deg. C/h
– Gradual changes in load resistance	± 20 % R_L

All changes in magnet current at frequencies of greater than 10 Hz are classified as ripple.

Design and Principle

The basic circuit diagram of the installations is shown in Fig. 2. Supply units of a similar design have been produced for a number of years. The principle is as follows:
The voltage from the three-phase network is applied through transformer T to the fully-controlled thyristor bridge A_1 to A_6. The d.c. voltage U_0 has a high harmonic content which is smoothed by the damped $L_F C_1$ low pass filter. The transistor control unit A_0 necessary for further reducing the ripple and compensating rapid changes in supply voltage is connected in series with the magnet. It comprises several water-cooled transistors connected in parallel (Fig. 3). The magnet voltage or current can be regulated by two independent controllers (thyristor or transistor control unit). Whereas the thyristor control unit has a control range of 0 to 100 %, the transistor unit has a range of only 10 to 20 % because of the working point losses. The control system comprises three partially intermeshed control loops, i.e. the U_{ce} regulator 1, the ripple controller 2 and the current regulator 3.
The U_{ce} *regulator 1* controls the thyristors such that the mean value of the voltage drop at the transistor control unit corresponds to the set mean value $U_{ce\,ref}$ remains constant. The working point is determined by the maximum deviations in supply voltage to be expected (5 %)

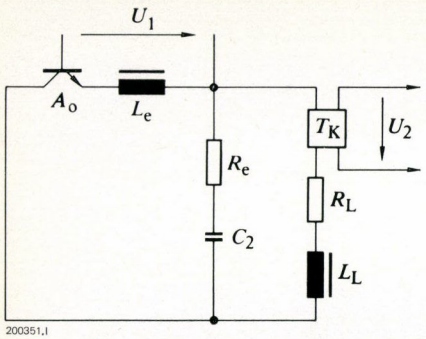

Fig. 4 – Equivalent circuit diagram of U_2/U_1 amplitude response

L_L = Load inductance
R_L = Magnet resistance

Other symbols, see text.

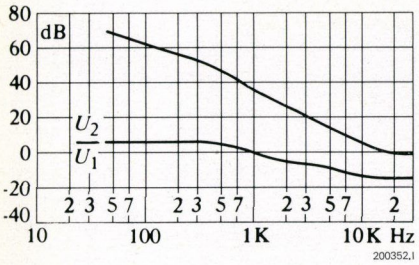

Fig. 5 – Amplitude responses according to Bode for the ripple regulator (measured values)

Top: Amplitude response of open regulator
Bottom: Amplitude response of control loop including transistor control unit

and the residual voltage ripple at the low pass filter. As an indirect function this control unit also performs the task of roughly adjusting the load voltage and controlling gradual fluctuations in supply voltage.

The *ripple regulating loop 2* reduces the interference values such as sudden changes in supply voltage, residual voltage harmonics from the low pass filter and the induced voltages at the magnet windings, as mentioned above.

The *current regulator 3* compares current I_{ref} at its input with the actual current value supplied by the precision d.c. transformer G_W and regulates the magnet current to the preset value by influencing its subordinate ripple regulator 2.

The current and ripple regulators (3 and 2) are responsible for supplying the required current source characteristic. The current regulator performs this function in the frequency range up to about 10 Hz. Its main task is regulating gradual changes in load. At higher frequencies the ripple regulator maintains zero fluctuation in current. The actual value transducer T_K for detecting current ripple forms the nucleus of this control loop and must have the following characteristics:

- the a.c. output signal at maximum permissible ripple (0·5 mA) must have a signal-to-noise ratio of at least 5:1,
- the cut-off frequency must be higher than 50 kHz and
- low d.c. losses.

Inductive circuits have the necessary properties for fulfilling these conditions and were also used in transducer T_K.

Amplitude Response of Ripple Regulator According to Bode

The equivalent circuit for determining the frequency response is shown in Fig. 4. The earth resistance R_e limits the earth current in the event of an earth fault. The capacitor C_2 between earth and the negative output terminal absorbs the commutation spikes and keeps them remote from the load. The capacitance between earth and the three-phase transformer introduces the commutation spikes in the power supply at each thyristor commutation. The choke L_e in the emitter circuit of the power transistors A_0 further reduces the harmonics by means of negative feedback. The stabilizing effect of the choke on the transistor control unit A_0 is an additional advantage.

Fig. 6 – Harmonic voltage U_e at passive filter with a load current of about 120 A

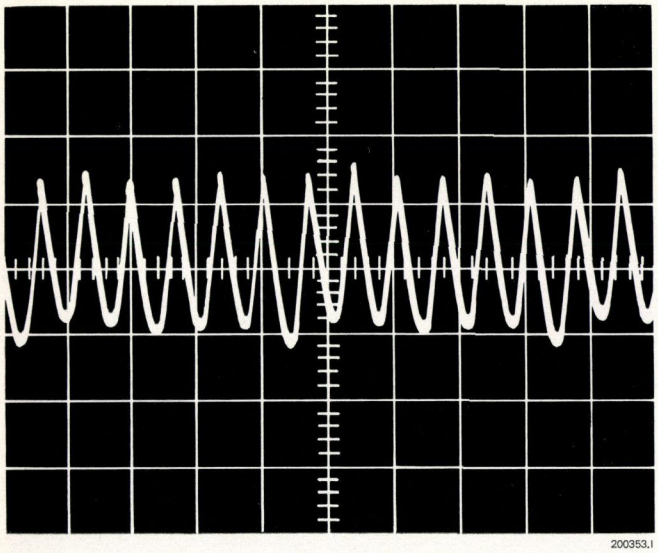

Fig. 7 – Ripple content in load current

Current scale: 0·7 mA/division
Time scale: 10 ms/division

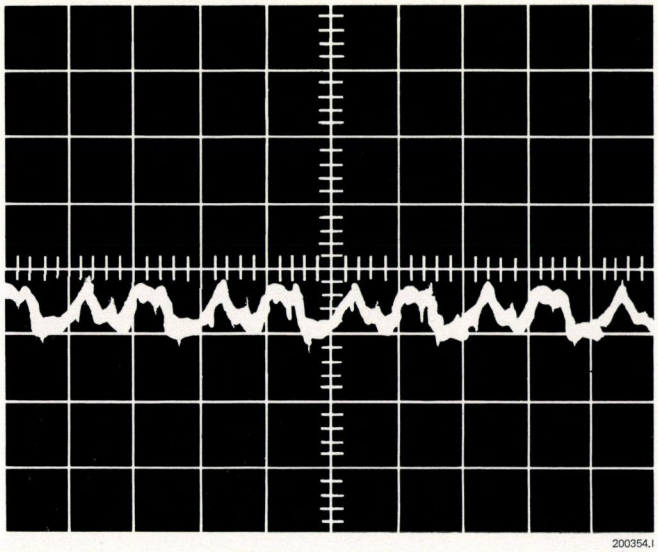

Figure 5 shows the amplitude responses for the control loop U_2/U_1 (Fig. 4) and of the complete ripple regulator (open loop including stabilizing element) according to Bode. The amplitude response of the open loop U_2/U_1 shows clearly the effect of the emitter coil L_e. Because of the effective negative feedback there is no voltage amplification at the transistor bank. Consequently the amplitude response is determined by the passive components alone and is easily stabilized.

In order to keep the costs of passive filters and the transistor control unit as low as possible it is essential to aim at a high regulator cut-off frequency. This is also essential for regulating the current fluctuations due to induced voltages on the load side.

A low-induction cable layout ensures a cut-off frequency of about 20 kHz necessary for attaining the required current ripple.

Transistor Control Unit, Passive Filter, Emitter Choke

These three power components, together with an optimum ripple regulator determine the reduction factor of the harmonics between the thyristor bridge and the magnet current. An economically optimum design resulted in the following values:

Low-pass filter:	$L_F = 11$ mH, $C_1 = 1{\cdot}5$ mF Damping of passive filter: 0·5
Transistor control unit A_0:	90 transistors (type 2N3773)
Emitter choke L_e:	1 mH, 135 A

Test Results

The current ripple was measured with a low-inductance resistance of about 140 mΩ and recorded on an oscillograph. The r.m.s. ripple measurement was carried out with an electronic r.m.s. value display instrument with amplified input signal. The induced voltage on the load side was simulated by means of an air-gap transformer with a 100 Hz oscillator.

Figure 6 shows the voltage ripple at the passive filter with a load current of about 120 A.

Figure 7 shows the corresponding load ripple current with an induced 100 Hz voltage of 20 V (r.m.s.). The total reduction factor at 100 Hz is approximately 20 times greater than at 600 Hz. For this reason the induced voltage was increased 10 times. The measured r.m.s. current value was 0·22 mA and comprises mainly the induced 100 Hz component.

The installations have been in operation for some considerable time and adequately fulfil the required guarantee requirements.

Conclusion

The test results show that the design chosen fulfils the requirements with fewer power components. A circuit with an active filter for overcoming the sudden $\pm$ 5% change in mains voltage would have been more expensive than the transistor control bank in spite of its higher power losses.

Coils with Inorganic Insulation and Their Application in Research Magnets

J. C. Rauch and E. Violi

Electromagnets used in particle accelerators and their experimental areas for focusing and deflecting charged particles are subject to intense radioactive radiation. Organic materials particularly are destroyed by this radiation; in the case of magnets this means the mostly organic insulation of the excitation coil. An alternative method of insulating these coils is described with special reference to a magnet of purely inorganic components produced for the Swiss Institute for Nuclear Research.

Introduction

At present, the majority of magnet coils have hollow or solid copper conductors with a mica/glass/epoxy insulation. Heat losses are dissipated by either direct or indirect forced water cooling or by the surrounding atmosphere. Glass/epoxy insulation systems known today have a resistance to radioactive radiation of 10^{10} rad [1, 2].
These radiation doses are reached within a year or even sooner in the vicinity of experimental targets. Consequently the coils of a magnet would have to be replaced frequently; however, because of the high radioactive half-life of certain materials used this involves special safety measures and also results in prolonged interruptions in experiments.

Fig. 1 – Section through a mineral insulated conductor

The conductor comprises a current-carrying inner copper bar which, depending on the cooling system, is either a solid (4) or hollow conductor (1) with compressed magnesium oxide powder for the insulation (3), and a continuous sheath of copper (2).

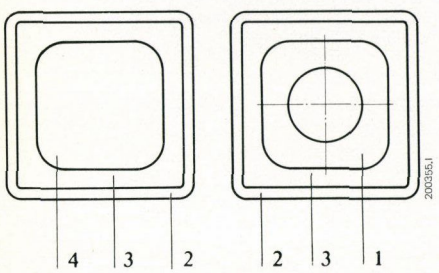

Coils with Inorganic Insulation

Continuous research is being carried out to find insulation systems which have greater resistance to radiation. Certain successes in this field are illustrated by impregnating the coils with silicon resins or concrete [3]. The 100 % inorganic and equally radiation resistant insulation with metal oxide powder tested at the Los Alamos Scientific Laboratory in New Mexico, USA, was particularly successful [4, 5].
The mineral insulated (MI) conductor, developed many years ago as a fireproof cable for monitoring equipment, is available today in square or rectangular cross section suitable for magnet coil manufacture. The conductor configuration is shown in Fig. 1.
The properties and tolerance of the conductor are determined by the manufacturing process. The final shape of the conductor is reached through several extrusion and drawing processes. The outside dimensions of the conductor are kept within very close limits by the draw bench, while the inner conductor, deformed by the highly compressed magnesium oxide powder, is relatively inaccurate. Consequently, the manufacturer can guarantee only the electrical resistance of the inner conductor per unit length and can give no guarantees for the cross section. Also, only a minimum resistance per unit length can be guaranteed between inner conductor and copper sheath.
Coils can be wound in the traditional manner using these conductors, which are available in various sizes. Where direct-cooled hollow conductors are used only a few tapes are required to hold them together. However, where indirect cooled solid conductors are used the turns must be soldered together to ensure adequate heat transfer. The maximum permissible temperature for the conductor in continuous operation is 250 °C but, in the case of hollow conductor coils, is kept below 100 °C by the cooling water. With indirect-cooled solid conductor coils this restriction is determined by the permissible temperature of the solder.
The dielectric strength of the insulation between the inner conductor and the sheath is 1·5 kV at 50 Hz for 1 minute. This value is ensured even if the conductor is greatly deformed (small bending radii) [4].
As the magnesium powder is highly hygroscopic special attention must be paid to the coil terminals. The conductor ends must be suitably protected against atmospheric moisture during the whole manufacturing process. The joints between two lengths of conductor should always be outside the coil. A coil wound with MI conductors has a poorer fill factor than a traditional coil.

Fig. 2 – Layout of the SIN laboratory

1 = Injector cyclotron
2 = Ring accelerator
7 = Target E
8 = Deflector magnet type AHE
13 = Experimental area πE1
18 = Area for μ experiments

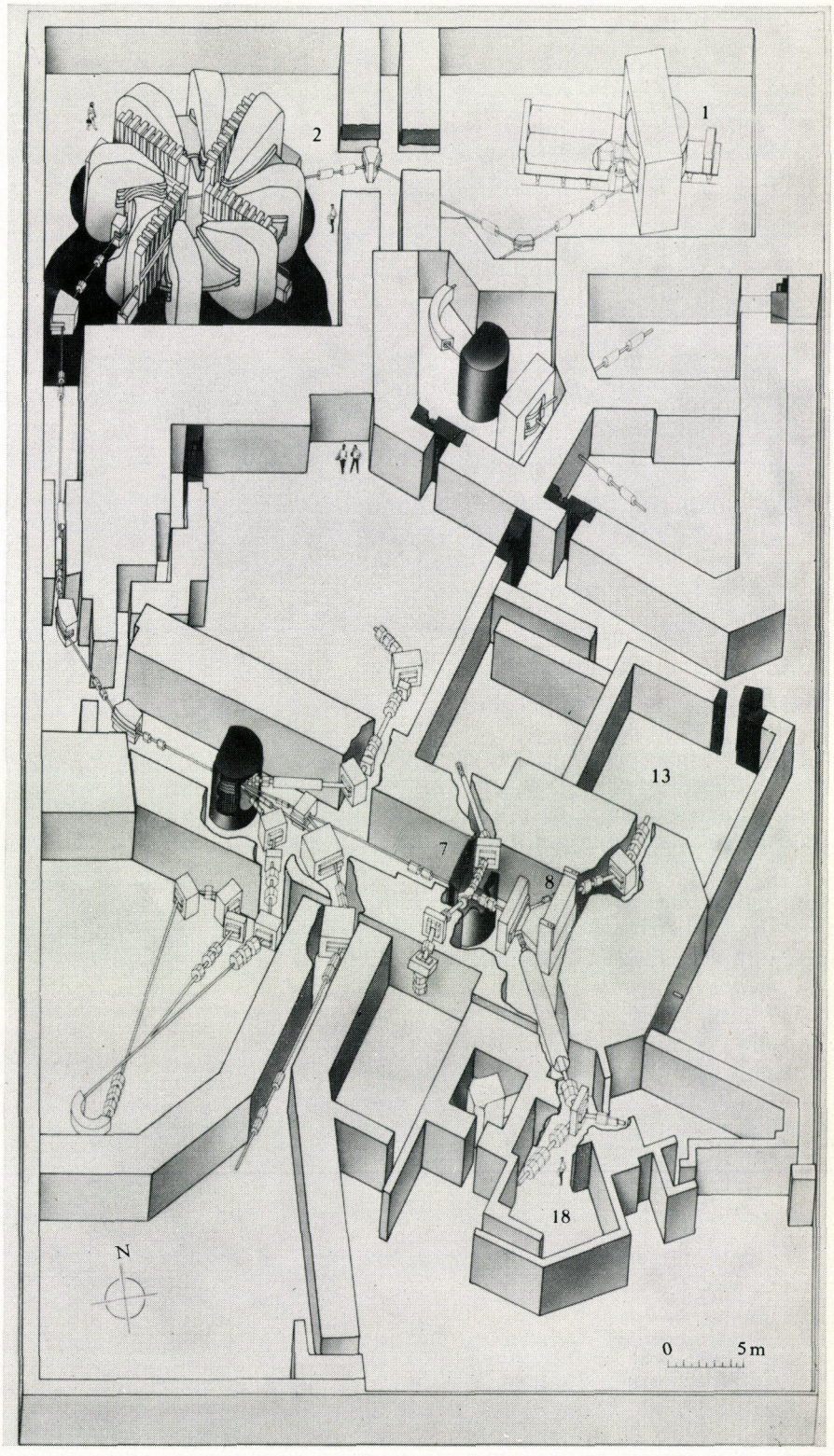

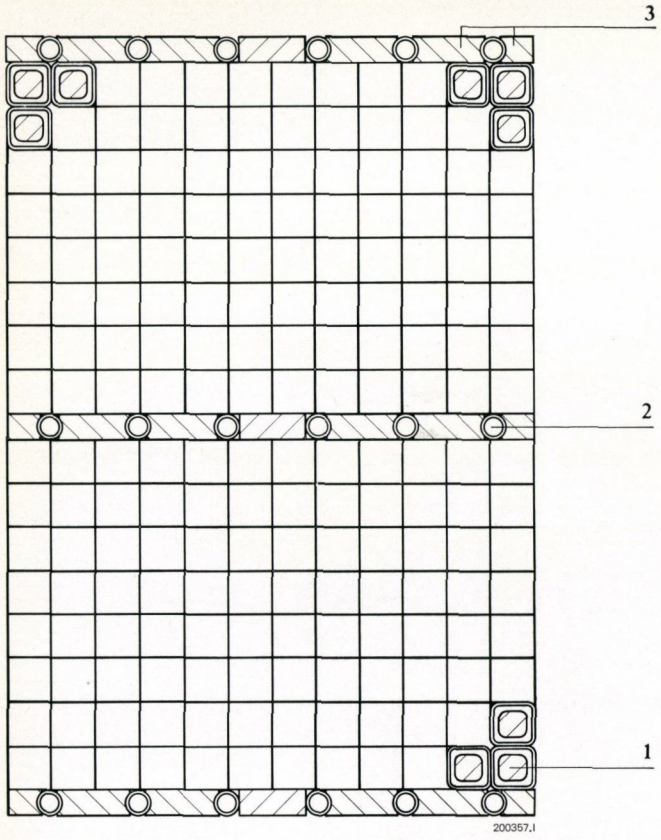

Fig. 3 – Section through one of the two coils of the AHE magnet

1 = Conductor with mineral insulation
2 = Cooling tubes of stainless steel
3 = Spacers

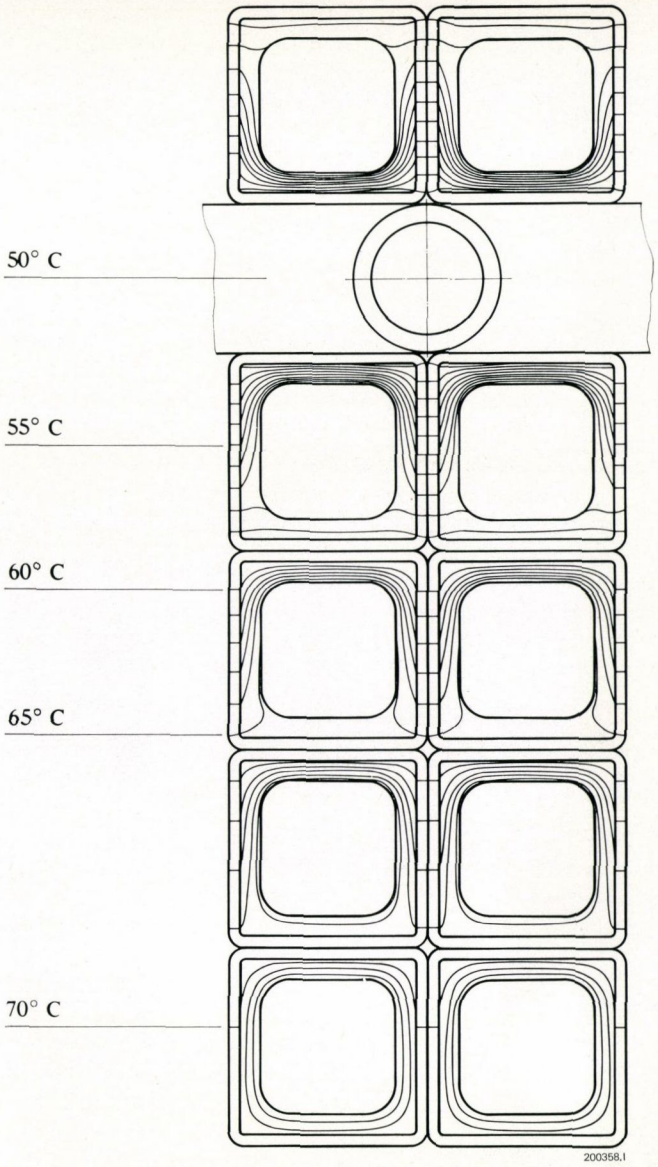

Fig. 4 – Calculated temperature distribution over the coil cross section

Type AHE Magnet with MI Coils

The type AHE deflector magnet described in the following is used in the Swiss Institute for Nuclear Research.
The location of the AHE magnet is clearly shown in the plan of the experimental laboratory (Fig. 2). The high-energy beams accelerated by the isochronous cyclotron 2 arrive at the thick target 7. The magnet 8 which deflects the beams to the experimental zones 13 and 18, is located immediately behind the target 7, i.e. in a zone where the radiation intensity is exceptionally high. For this reason the coils have mineral insulation.
The basically simple, H-shaped deflecting magnet makes stringent demands with respect to field homogeneity and radiation resistance properties. A collimator mounted in the vacuum chamber gives it its unusual form.

Data of the AHE Magnet

Air gap	δ	= 180 mm
Pole length	l	= 650 mm
Magnetic field	B	= 1·3 T
Outside dimensions of yoke		1130 × 1960 × 3080 mm
Current	I_{max}	= 545 A
Power consumption	P	= 165 kW
Indirect water cooling		
– with a water flow rate	Q	= 2 l/s
– with a pressure drop	Δp	= 7 bar
Water temperature rise	$\Delta\vartheta$	= 20 deg. C
Weight	m	= 40 t

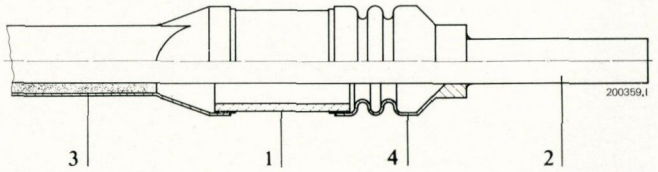

Fig. 5 – Air-tight, soldered seal for conductor ends

This seal, developed by Brown Boveri (patent applied for), comprises a ceramic tube 1 forming the insulation between the inner conductor 2 and the sheath 3, a compensating bellows 4 which takes up the difference in expansion between the inner conductor and the sheath. The components are soldered together. One end of the ceramic tube is soldered direct onto the expanded sheath.

Coils

The coil cross section is shown in Fig. 3. Each of the two coils has 192 turns divided into four sections interconnected outside the radioactive zone. The layers of stainless steel cooling tubes can be seen at top, centre and bottom.

Fig. 6 – Tin-impregnated coil

The finished coil unit, complete with spacers and supports, is absolutely self-supporting and withstands all magnetic and thermal forces occurring under test and operating conditions.

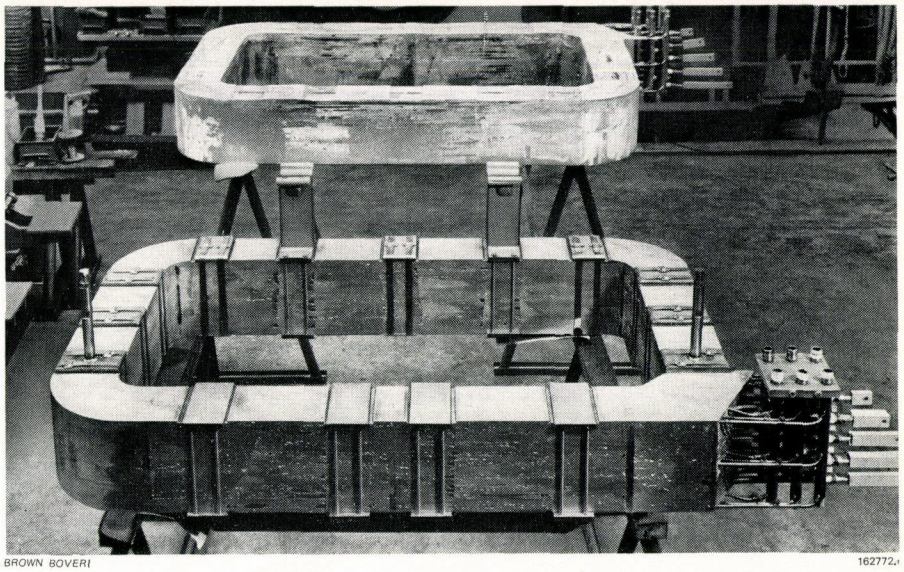

This arrangement was chosen because, on the one hand, a relatively high current density (approx. 3 A/mm² over the cross section) was achieved and, on the other, the demineralized radioactive water must not be allowed to come into contact with copper (corrosion) as would have been the case with a hollow-conductor coil.

Mineral insulated conductors are exceptionally well suited for coils with indirect cooling because the heat dissipation is promoted by the copper sheath of the conductor. In contrast to a normally insulated coil there is only one heat transfer through the insulation and the copper sheaths which are soldered to each other. The calculated temperature distribution over the coil cross section is shown in Fig. 4. The temperature difference between the cooling water and the hottest spot is about 20 deg. C. For safety reasons the cooling system is designed for ample cooling capacity.

The mineral insulated conductor has outer dimensions of 13·5 × 13·5 mm and the inner conductor is 8·5 × 8·5 mm. The conductors were supplied in 120 m lengths, were tin plated and wound in double pancakes. The conductor ends were fitted with soldered seals (Fig. 5). These end seals fulfil all requirements regarding radiation resistance, endurance strenght and dielectric strength.

The double pancakes, together with the preformed cooling system, were installed in a mould and, when the necessary precautionary measures had been carried out, they were impregnated with pure tin. Tests confirmed the excellent soldering bond between the conductors. The finished coil is shown in Fig. 6.

Iron Core

In order to comply with the set requirements in respect of field homogeneity a filter gap was provided between each pole and yoke. The filter gap, which has been used successfully in other magnets, permits distortion in the field curves to be reduced; also, the two poles, together with the accurately machined spacers, can be bolted together to form a pole unit (Fig. 7) in order to maintain the required co-planarity of the pole faces under various operating conditions.

The size of the pole faces would have required very thick or reinforced walls for the vacuum chamber. In order to eliminate this drawback an integrated vacuum chamber was installed, i.e. a vacuum chamber where the upper and lower walls are formed by the pole faces. This system has already been successfully applied in the sector magnets of SIN and in the 600 and 900 spectrometer magnets for CEA in Saclay.

Producing an integrated vacuum chamber involves perfect, leak-proof welded joints between stainless steel and the special low-carbon magnet steel; work which can be carried out only by trained staff with wide experience, and which relies on extensive testing.

Fig. 7 – Vacuum chamber and pole unit for the AHE magnet

The structure at the right-hand end of the vacuum chamber is for mounting a collimator.

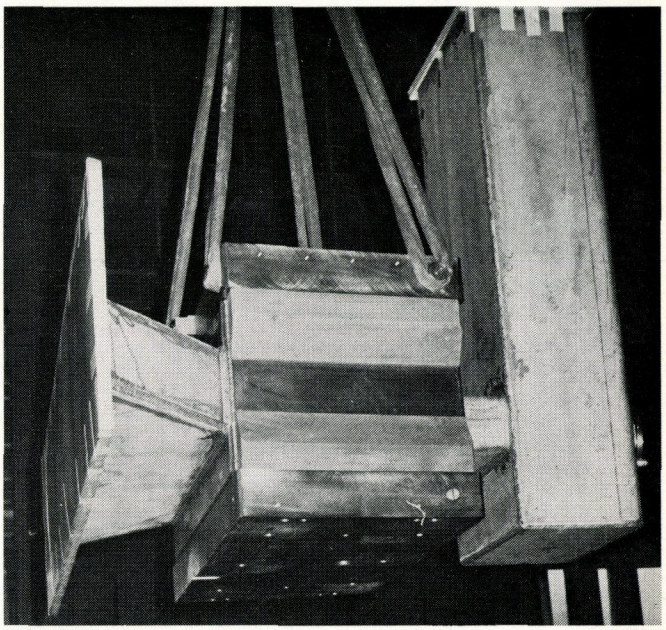

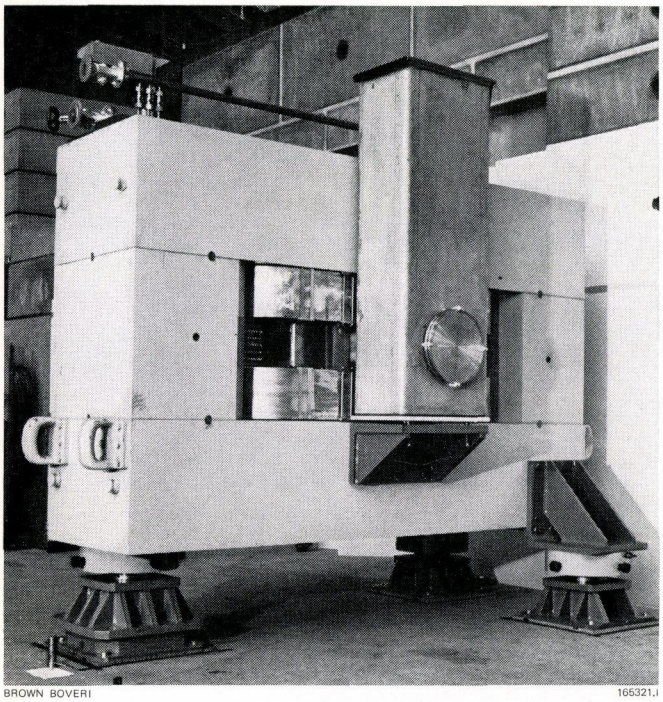

Fig. 8 – Type AHE magnet in the SIN laboratory

The Assembled Magnet

To facilitate rapid dismounting in a highly radioactive environment, there are no screwed fixings between any of the components. The yokes and pole unit are dowelled and the coils are separated and supported from the pole by bushings and spacers. The hydraulic connections and electrical terminals for the coils are located at a metal console and can be dismounted together with the coils.
The electrical connections are supported on ceramic insulators. The hydraulic connections and water manifold are of stainless steel. The temperature monitoring for the cooling circuits is carried out by glass and ceramic insulated thermal switches connected by ceramic insulated straps to a ceramic terminal strip.
Figure 8 shows the magnet installed in the SIN laboratory.
Installation was carried out without any noticeable difficulties by our own staff. Commissioning and testing was carried out to the fullest satisfaction of the client.

Bibliography

[1] *M. H. van de Voorde:* Improvements in the properties of organic materials in accelerator magnets. Third International Conference on Magnet Technology, Hamburg, May 1970.

[2] *M. H. van de Voorde:* Effects of radiation on materials and components. Lecture given in the Academic Training Programme of CERN 1968–1969.

[3] *H. F. Vogel, J. J. Rosenthal:* Cement potted coils for muon channel magnets. Los Alamos Scientific Laboratory, Private communication.

[4] *A. Harvey:* Mineral-insulated conductors for magnet coils. Private communication.

[5] *A. Harvey, S. A. Walker:* Mineral-insulated magnets for high-radiation environments. IEEE Trans. Nuc. Sci. NS-16, No. 3, 611–612, June 1967.

In Brief

AAS Veritron—A New Range of Three-Phase, Two-Way Static Convertors

G. Sola

General

For many years now Brown Boveri have produced static convertors for supplying d.c. machines used in industry. The new range of AAS Veritrons (Fig. 1) increases the range of models towards the lower power applications, providing a more compact, improved version of two-way Veritron static convertor carrying circulating current and with inverse pairs of thyristors.

AAS Static Convertors

Type AAS Veritron static convertors, whose basic circuit diagram is shown in Fig. 2, are designed for supplying d.c. machines rated up to 40 kW for motoring and braking in both directions of rotation.

The main features of this equipment are excellent control response and, particularly, their capacity for rapid and continuous current reversal with no dead intervals. These features are essential for those control tasks where exact guidance is required at very low speeds or under no load.

As a result their main applications are:

- feed drives for machine tools,
- reversing drives for test machinery, and
- drives which are controlled to zero speed while producing a torque.

Basically this equipment comprises a power section and a Verimat control unit.

The inverse pairs of thyristors in two star connections form the power section. Both star connections, of which the one operates as a rectifier and the other as an inverter, operate simultaneously resulting in instantaneous current reversal. The circulating current flowing between the two star connections is limited by reactor coils.

The Verimat control equipment comprises two reversible printed circuit boards which can be removed through the front, thus simplifying commissioning and maintenance.

The AAS thyristor static convertors are available for 380 V/3-phase, 50 or 60 Hz, or 500 V/3-phase, 50 Hz. The main data of the various types is listed in Table I.

Table I: Main data of the new range of three-phase, two-way static convertors, type AAS

Type	Supply voltage V	Motor voltage V d.c.	Continuous current A d.c.
AAS 1101	380 V/3-phase	200	17
AAS 1201	50 or 60 Hz		25
AAS 1301			36
AAS 1401			60
AAS 1501			80
AAS 1601			105
AAS 1701			125
AAS 1801			170
AAS 1451	500 V/3-phase	260	60
AAS 1551	50 Hz		80
AAS 1651			105
AAS 1751			125
AAS 1851			170

Fig. 1 – Veritron two-way static convertor type AAS
Supply voltage: 380 V/3-phase
Motor voltage: 200 V d.c.
Continuous current: 36 A d.c.

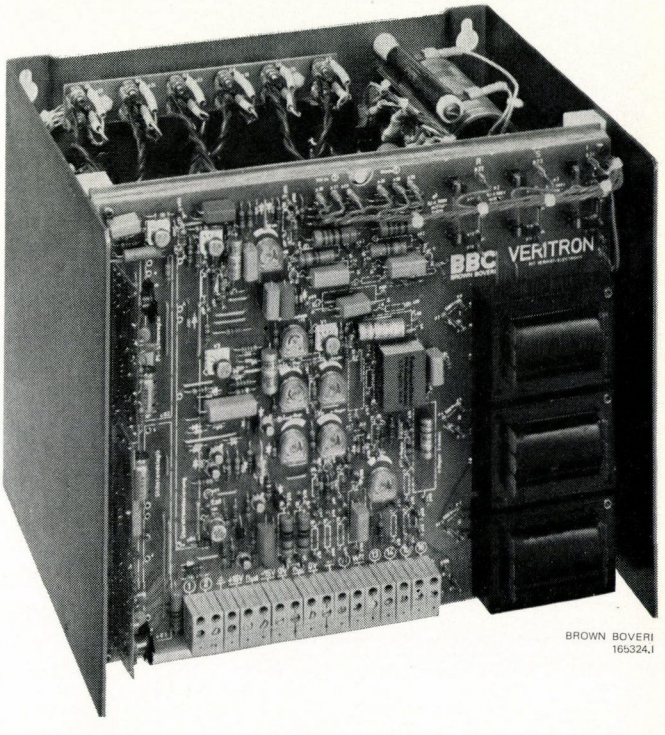

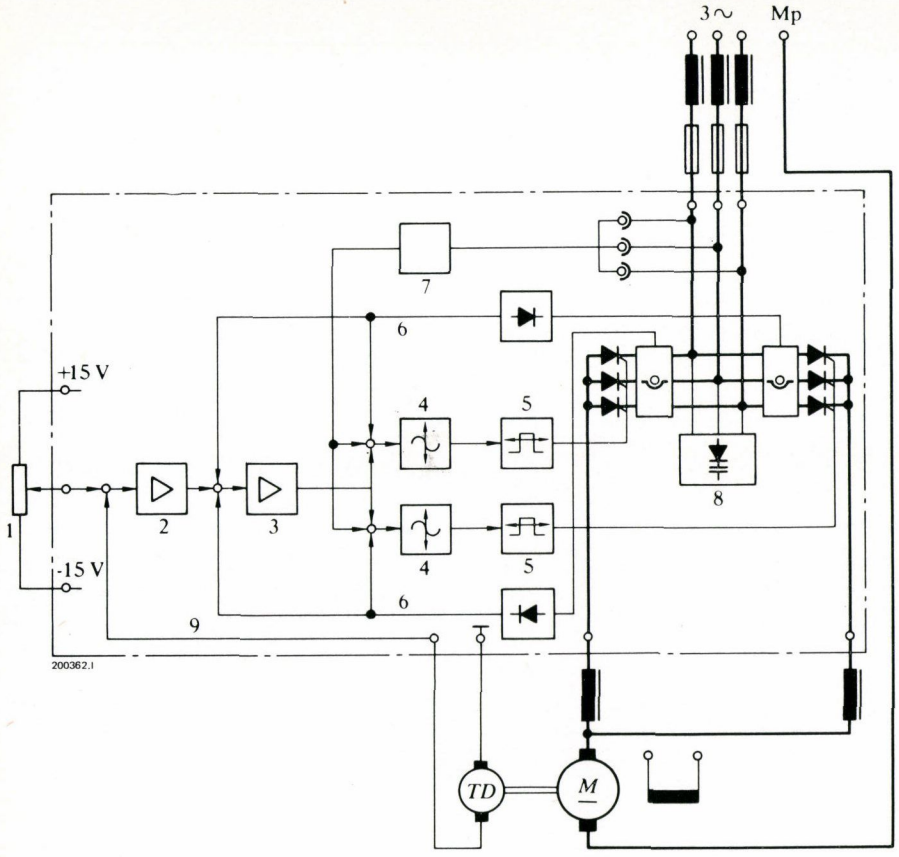

Fig. 2 – Block circuit diagram of a two-way static convertor type AAS

1 = Speed set point
2 = Speed controller
3 = Current controller
4 = Sine signal generator
5 = Pulse generator
6 = Actual current value
7 = Switching logic
8 = Overvoltage protection
9 = Actual speed value

Table II: Overall range of Veritron static convertors

Series	Power range kW	Features	Type of duty	Speed range	Design
GCB	0·9–9	Semi-controlled single-phase bridge	Direct drive	1:100	Compact design, electronics on front panel
GSB	2·1–9	Fully-controlled single-phase bridge	Reversing drive with rotor reverser type GV 7601 or anti-parallel connection with circulating current	1:100 1:500	Compact design, electronics on front panel
ASD	7·5–90	Fully-controlled three-phase bridge	Direct drive Reversing drive by anti-parallel connection with circulating current	1:300	Compact design, electronics on front panel
AAS	3·4–34	Anti-parallel star connection with circulating current	Reversing drive	1:5000	Compact design, electronics on front panel
CSD	11–1500	Fully-controlled three-phase bridge	Direct drive Reversing drive by anti-parallel connection with circulating current	1:300 1:500	Electronics in modules
CKD	18–1400	Fully-controlled three-phase bridge with contactor changeover	Reversing drive	1:300	Electronics in modules
CAD	18–1400	Three-phase bridge in anti-parallel connection without circulating current	Reversing drive	1:300	Electronics in modules

Optional Equipment

The optional equipment comprises printed circuit boards which can be installed in the Verimat control system. They are for various monitoring and control functions as described in the following.

Zero Speed Logic

The zero speed logic p.c.b. supplies an electronic signal at the instant that the set point and actual value of the speed simultaneously reach a value in the region of zero. This signal can be used, for instance, for controlling a mechanical brake.

Overcurrent Apportioning

This equipment permits dynamic current control. Various types of operation, e.g. servo-motors, require current during acceleration or deceleration which, for a short time, may be several times the rated current of the static convertor. Dynamic current limiting enables thermal overloading of the equipment to be avoided in these applications.

P Adaptation

As shown in Fig. 2 this alters the gain of the current regulator with respect to the current value. At low values the gain is increased resulting in a broader control range and improved dynamic response of the drive at low speeds.

Application

The AAS thyristor static convertors were designed specially for drives which require highly accurate speed control, a broad control range (values of 1:5000 are attainable) and very good dynamic response. The range of the Veritron static convertor for reversing drives and low powers is thus conveniently increased by the type AAS models. The whole range of Veritron equipment is compiled in Table II.

BBC
BROWN BOVERI

BBC Brown, Boveri & Company, Ltd.
Baden/Switzerland